Cytotoxicity of Mn-based photoCORMs of ethynyl-α-diimine ligands against different cancer cell lines: The key role of CO-depleted metal fragments

Jeremie Rossier [1], Joachim Delasoie [1], Laetitia Haeni [2], Daniel Hauser [2], Barbara Rothen-Rutishauser [2,*] and Fabio Zobi [1,*]

[1] Department of Chemistry, University of Fribourg, Chemin du Musée 9, 1700 Fribourg, Switzerland.
[2] Adolphe Merkle Institute, Chemin des Verdiers 4, 1700 Fribourg, Switzerland.
* Correspondence: fabio.zobi@unifr.ch

Received: date; Accepted: date; Published: date

Abstract: A series of *fac*-$[Mn(CO)_3]^+$ complexes bearing 4-ethynyl-2,2'-bipyridine and 5-ethynyl-1,10-phenanthroline α-diimine ligands were synthetized, characterized and conjugated to vitamin B_{12}, previously used as a vector for drug delivery, to take advantage of its water solubility and specificity toward cancer cells. The compounds act as photoactivatable carbon monoxide-releasing molecules (photoCORMs) rapidly liberating on average ca. 2.3 equivalents of CO upon photo-irradiation. Complexes and conjugates were tested for their anticancer effects, both in the dark and following photo-activation, against breast cancer MCF-7, lung carcinoma A549 and colon adenocarcinoma HT29 cell lines as well as immortalized human bronchial epithelial cells 16HBE14o- as the non-carcinogenic control. Our results indicate that the light-induced cytotoxicity these photoCORMs can be attributed to both their released CO and to their CO-depleted metal fragments (i-photoCORMs) including liberated ligands.

Keywords: carbon monoxide; photoCORMs; breast cancer MCF-7; lung carcinoma A549; colon adenocarcinoma HT29

1. Introduction

Carbon monoxide (CO) is produced in several mammalian tissues by the heme oxygenases (HOs) family of enzymes following the catalytic degradation of heme and has multiple physiological roles [1-4]. The inducible HO isoform (HO-1) and its constitutive isoform (HO-2) are enzymatically active in the presence of oxygen and depend on NADPH. Some of the known effects that CO triggers physiologically include antiproliferative, anti-inflammatory, antiapoptotic and anticoagulative responses, however, at high concentration, the molecule causes acute systemic toxicity [2-4]. It is noteworthy that HO-dependent CO production can be inhibited by several small chemical molecules such as mesoporphirins, typically Zn deuterpophyrin (ZnDP), or protoporphyrins (PP) such as ZnPP or SnPP [1-4].

Several types of tumors contain high level of HO-1 implying that cancer cells physiology is heavily dependent on CO [5]. Generally speaking, at low concentration, CO administration is reported as mainly inducing pro-proliferative and pro-angiogenic effects on tumors while at higher concentration, administration of CO or CO releasing molecules (CORMs) leads to reduced cell viability [4]. The functional importance of low CO concentration on cancer cell viability is inferred mainly by HO-1 silencing experiments. siRNA-mediated suppression of HO-1 leads to decreased viability of pancreatic cancer *in vitro* and *in vivo* [6]. Likewise, by silencing HO-1, it was shown that mouse hepatoma cell lines grew slower than the tumor expressing normal levels of HO-1 [7]. The use of HO-1 inhibitors on tumor-bearing mice could further highlight a reduced growth of several implanted tumor [8-10]. Furthermore, the approach of inhibiting HO-1 to reduce the cytoprotective and pro-proliferative effects of CO is supported by several preclinical data [11-13]. However, a few other studies have reported that, following HO-1 inhibition, tumor growth increased, implying an anti-proliferative action of CO [14, 15]. While it is clear that the functional biochemistry of HO-1 goes beyond the physiological production of CO, this evidence has led to the hypothesis that the effects of HOs and low CO concentration in tumors might be highly cell-type dependent [14, 15].

High intracellular concentration of CO or HO-1 hinders cancer cell viability, presumably *via* an anti-Warburg effect by rapidly fueling cancer cell bioenergetics, inducing metabolic exhaustion [16]. Typically, CO gas administrated to tumor-bearing mice (250 ppm for 1 hour per day) leads to an increase of apoptosis and a reduced vascularization in cancer xenografts.[16] Similarly, CAPAN-2 pancreatic cancer cell growth and angiogenic response were reduced following CO administration (500 ppm per for 1 hours per day) [17]. Interestingly, these results were equated by administrating the CO releasing molecule CORM-2, intraperitoneally at a dosage of 35 mg/kg/day [17]. This latter compound, which offers the advantage of providing CO in the solid state, has been used profusely in preclinical studies and has led to the development of numerous CORMs in this field of research [3, 18].

Indeed, photoactive metal carbonyl compounds able to release CO (known as photoCORMs) have gained momentum over the past few years regarding their potential use against cancer [19-21]. *In vitro* experiments, conducted by the group of Mascharak [22-25], have shown that manganese-based complexes bearing azopyridine-type ligands could eradicate about 40% of an MDA-MB-231 breast cancer colony at a concentration of 75 μM upon visible light irradiation [26]. Similarly, about 50% of cell death occurred under light exposure of the compound *fac*-[MnBr(CO_3(pbt)] at 100 μM, which could be tracked intracellularly following the light-induced release of its 2-(2-pyridyl)benzothiazole (pbt) ligand [27]. The effects of these, and similar photoCORMs, are attributed to CO-mediated attenuation of glutathione and nuclear metallothionein levels [28] and inhibition of cystathionine β-synthase [29]. Similarly, prostate cancer cell's, (PC-3), viability was reduced by approximately 60% following light-triggered CO release of the [Fe(CO)(N_4Py)](ClO_4)$_2$ complex at a concentration of 10 μM [30]. Schatzschneider has used the compound *fac*-[Mn(CO_3(tpm)]PF_6 to reveal a significant photoinduced cytotoxicity comparable to that of established 5-fluorouracil (5-FU) in HT29 colon cancer cells [31]. Kunz could not directly observe any cytotoxicity induced by the release of CO on Hct116 human colon carcinoma and HepG2 human hepatoma cells by using *fac*-[Mn(CO_3] complexes of bpma-type ligands grafted on polymers [32]. Other author also reported similar observations [33, 34] highlighting the complexity of the subject, as discussed elsewhere [35, 36]. Indeed, an ongoing issue is the formation and accumulation of toxic products following CO and ligand release from the metal center, as it was shown for the well-known CORM-2, whose CO-depleted molecule was found to have a cytotoxic activity by its own [37]. Furthermore, in the case of some photoCORMs, typically the ones featuring a Re metal core, the formation of ROS could also play a key role and prevent a direct interpretation of the results regarding the role of CO [38].

While investigating the targeted prodrug delivery of organometallic anticancer derivatives via transcobalamin-mediated uptake [39], we prepared a *fac*-[Mn(CO_3]$^+$ complex with 4-ethynyl-2,2'-bipyridine and observed unusual dark and light-induced cytotoxicity. The complex, which was omitted from the study above, served as a blueprint for the design of a series of photoCORM complexes which we have studied and present here along their vitamin B_{12} conjugates. Given the hypothesis that the effects of CO on cancer cell viability are highly cell-type dependent, we addressed the cytotoxicity of the series of molecules against three different cancer cell lines and compared the results with the effect observed by using cells derived from a healthy tissue. Breast cancer MCF-7, lung carcinoma A549 and colon adenocarcinoma HT29 cell lines were selected as cancerous tissues while immortalized human bronchial epithelial cells 16HBE14o- served as non-carcinogenic controls. In this contribution, we report the investigation of the dark and light-induced cytotoxicity of this series of Mn-based photoCORMs bearing ethynyl-α-diimine ligands. Overall, our results indicate that, dissimilarly from the well-established species described by other authors, light-induced

cytotoxicity these photoCORMs can be attributed to both their released CO and to their CO-depleted metal fragments (i-photoCORMs), including liberated ligands.

2. Results and Discussion

2.1. Compounds synthesis and characterization

Manganese(I) complexes bearing a terminal alkyne Mn-**1** to -**4** (Fig. 1 and 2) were obtained in high yields from the reaction between [$MnBr(CO)_5$] and the corresponding α-diimine ligands following a general procedure. In each case, suitable single crystals were grown from diffusion of hexane into concentrated dichloromethane solutions. The molecular structures of the set shown in the Fig. 1 were determined by X-ray analysis. The structural parameters reveal that the manganese centers reside in a distorted octahedral symmetry which is more pronounced in the case of compounds Mn-**3** and -**4** owing to the influence of their ortho-substituted ligand (Me_2bpy and Me_2phen). The *fac*-$[Mn(CO)_3]^+$ core nature of the compounds is also confirmed by the analysis. Indeed, the equatorial planes consist in two C atoms of the CO groups and the two N atoms from the bidentate ligands, while the axial plane is occupied by the bromide and the last CO.

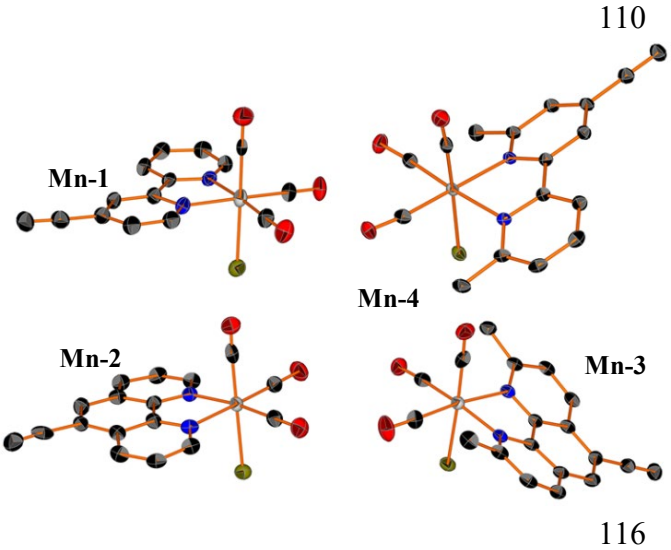

Fig. 1 X-ray molecular structures of the Mn^I complexes used in this study (thermal ellipsoids are shown at the 50% probability).

Complexes Mn-**1** to -**4** were then attached to a cobalamin scaffold directly through the alkyne functionality. The reason for preparing these species was dictated by previous findings which showed that these conjugates take advantage of the vitamin water solubility, active uptake and specificity toward cancer cells and their general lower toxicity [39]. The latter in particular was anticipated as a useful property in providing a handle to fine-tune compounds based on their IC_{50} values for this study. The copper-mediated synthesis of the alkylated vitamin B_{12} derivatives,

presented in Fig. 2, relies on a previously established procedure that was adapted to our needs [40]. Typically, the reaction yields between 70 and 90% but derivative B_{12}-Mn-**3** could only be obtained in a moderate 50% yield, presumably because of the low solubility of Mn-**3** in the reaction solvent. The ^{1}H-NMR spectra of the derivatives are consistent with the diamagnetic ground state of both Co^{III} and Mn^{I}. A closer look at the aromatic region of the spectra, as shown in Fig. 3, indicates of the successful preparation of the cobalamin conjugates.

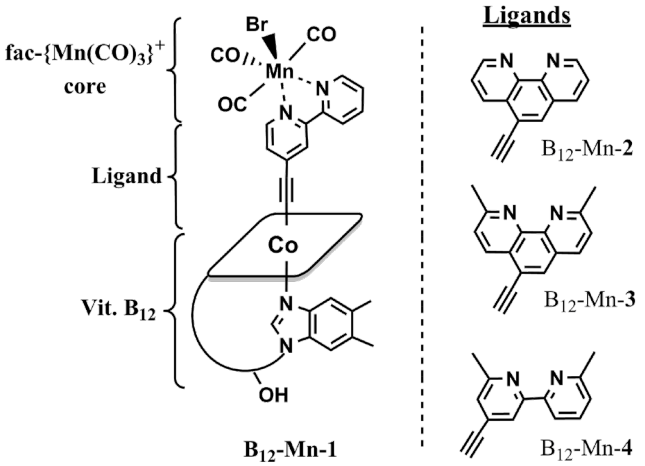

Fig. 2 Structures of the B_{12}-Mn-**1** to -**4** photoCORMs

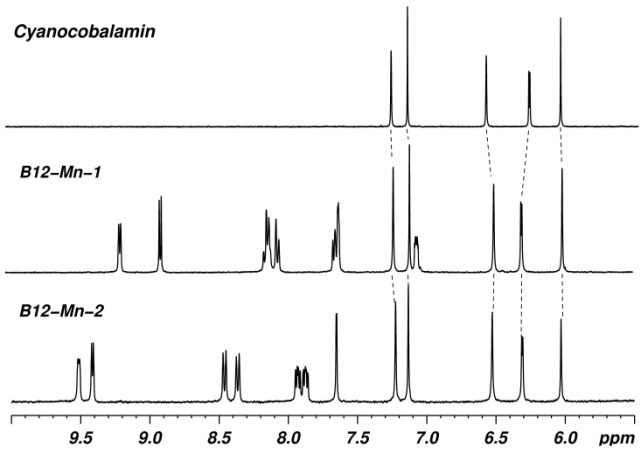

Fig. 3 Aromatic region of the ^{1}H-NMR spectra (500 MHz, D_2O) of cyanocobalamin and of the derivatives B_{12}-Mn-1 and -2. The dotted lines follow the signals belonging to the cobalamin scaffold. All signals referenced to residual solvent peak.

In our analysis, spectra of B_{12}-Mn-**3** and -**4** revealed a doubling of some aromatics signals. As a matter of fact, the highly distorted symmetry of complexes Mn-**3** and -**4** might explain this observation. Indeed, interaction between the corrin ring and the methyl groups of the α-diimine ligands could be sterically disfavored and prevent the Co-C_{sp} bond to freely rotate as previously observed [41]. This hypothesis was supported by temperature-depended measurements (ESI). From

a stability point of view, Mn-**1** to -**4** and their B_{12} derivatives were stable for at least 7 days in water, protected from light as well as 48 hours in the respective cell culture media used. However, a thermal decomposition occurred consistently between 60 and 70°C.

2.2. CO-releasing properties of the compounds

The absorbance spectra of complexes Mn-**1** to -**4** display a broad band in the 350 nm – 450 nm range which was correlated to MLCT transitions for similar analogues [42, 43]. Their maxima show very little differences (~420 nm ± 15 nm) and were deemed suitable for visible light irradiation. The spectra of the B_{12} derivatives are less indicative of the presence of the Mn^{I} complexes since electronic transitions of the B_{12} scaffold overshadow the MLCTs. However, under exposure to visible light using a 10W power white LED to which a 420 nm wavelength filter was applied, an obvious change occurs rapidly in all cases. The change is characterized by the almost complete disappearance of the MLCT band for the manganese complexes. In the case of the B_{12} species B_{12}-Mn-**2** to-**4**, the α and β bands were found to merge following irradiation suggesting the formation of more than one B_{12} photoproduct. The photolysis of the CO ligands can be probed by IR spectroscopy and is representative of the extent of reaction (see ESI). The absorption frequencies attributed the symmetrical and asymmetrical vibrations of the metal-tricarbonyl moiety gradually disappear following 20 seconds irradiations lapses in methanolic solutions containing pure vitamin derivatives suggesting that close to three carbonyls are being released under these conditions. The alkyne frequencies, however, remain relatively unchanged. These observations were further confirmed by mass analysis of the solutions. Indeed, the presence of the photoproduct B_{12}-[MnBr[N^N](solv)$_3$] alongside with the B_{12} bound to the α-diimine ligands lacking the *fac*-$[Mn(CO)_3]^+$ core was systematically observed. Ultimately, we were able to grow single crystals of the manganese-free photoproduct B_{12}-**bpy** formed following the irradiation of B_{12}-Mn-**1**. The molecular structure (Fig. 4) reveals a slightly bent Co-C≡C angle (179.24°) and a triple bond (1.196 Å) longer than in organic alkynes, which is consistent with recently reported acetylide cobalamins [40, 44].

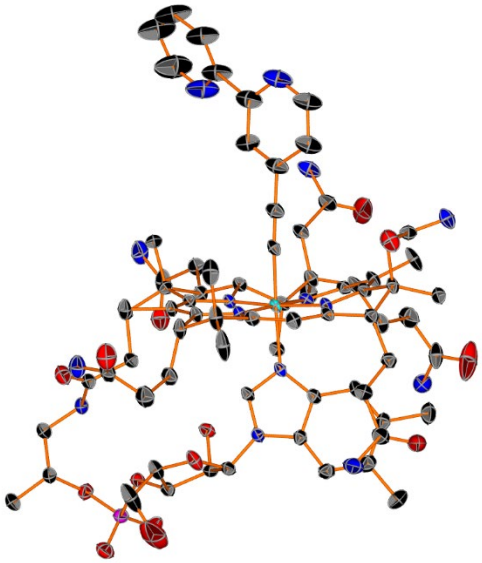

Fig. 4 X-ray molecular structure of the photoproduct B12-**bpy** (thermal ellipsoids are shown at the 50% probability).

The pseudo half-lives and equivalents of CO release from compounds Mn-**1** to -**4** and B_{12}-Mn-**1** to -**4** were determined by monitoring the changes in the UV-Vis spectrum at wavelengths corresponding to the absorption maxima of the free Mn^{I} complexes in PBS and are listed in table 1. CO release is very fast and is independent of α-diimine ligand used within the free and B_{12} conjugated series of compounds. The photoinduced carbon-monoxide-releasing properties of the photoCORMs were further evaluated under the conditions of the myoglobin assay (0.1 M PBS pH 7.4, 60 uM Mb, sodium dithionite 10 mM, Ar atmosphere). Prior to each experiment, the stability of each compound in the presence dithionite was evaluated and none of the complexes showed spontaneous CO release.

In the assay, the changes in the 550 nm region are indicative of the formation of CO-Mb (see ESI). Furthermore, the equivalents of CO release per molecule of photoCORM seems to be independent of the structural changes in the rigid α-diimine ligands. Via this method, on average, 2.3 equivalents of CO were calculated as being released by the molecules (table 1). Taken together, the results indicated that our designed photoCORMs could be considered for further use to deliver CO to biological target under physiological conditions.

193 **Table 1.** Kinetic data of photo-induced CO-release of the compounds tested in this study

	$^{p}t_{1/2}$ [sec][a]	equiv. of CO released[b]
Mn-1	2.3 ± 0.1	1.45 ± 0.03
Mn-2	3.31 ± 2.30	2.3 ± 0.02
Mn-3	5.65 ± 1.0	n.d.[c]
Mn-4	3.46 ± 0.1	2.49 ± 0.02
B_{12}-Mn-1	12.9 ± 0.6	2.26 ± 0.06
B_{12}-Mn-2	13.7 ± 1.5	2.74 ± 0.13
B_{12}-Mn-3	15.8 ± 1.9	2.20 ± 0.05
B_{12}-Mn-4	13.3 ± 1.4	2.39 ± 0.09

194 a. Pseudo half-life, determined from UV/Vis spectral studies b. determined under the conditions of the
195 myoglobin assay c. Not determined due to the general poor solubility of Mn-**3**

196

197 *2.3. Cellular uptake mechanism of B_{12}-photoCORMS*

198 Vitamin B_{12} (Cbl), is an essential vitamin which is carried through systemic circulation by
199 cobalamin-binding proteins. Ultimately, the transcobalamin-bound Cbl is internalized in cells
200 following a receptor mediated endocytosis, a feature which was previously exploited to target cancer
201 tissues [39, 45, 46]. This uptake mechanism differs from the passive diffusion which characterizes
202 most of the manganese tricarbonyl complexes reported to date. By comparing the two sets of
203 compounds, the free and the vitamin bound manganese complexes respectively, we aimed to
204 understand whether different cellular pathways could influence the cellular response triggered by
205 the photoCORMs.

206 To take advantage of this active transport, modifications at the upper side of the cobalt or at 5'-
207 sugar carbon of the vitamin are tolerated if they don't induce structural changes to the corrin ring
208 [47]. Therefore, to investigate the uptake mechanism of our B_{12} photoCORMs, compound B_{12}-Mn-**1**
209 was labeled at the sugar moiety with rhodamine as previously described [47]. Human bronchial
210 epithelial cells 16HBE14o- were then incubated with the compound for 30 min at 37°C and at 4°C in
211 two separate imaging chambers and laser scanning microcopy was used to probe the uptake of the
212 fluorescent Cbl. The result shows a clear difference between the two conditions of incubation as
213 shown in the Fig. 5. At 37°C, the fluorescence of the compound is clearly found inside the cell, but
214 mainly outside the nucleus and testifies of the cellular uptake of the derivative. However, at 4°C
215 where active processes are inhibited, minor intracellular fluorescence could be observed. Taken
216 together, these results constitute evidence that the cobalamin derivatives (i.e. B_{12}-Mn-**1** to -**4**) are being

actively transported while passive diffusion is assumed for Mn-**1** to -**4** complexes under similar conditions.

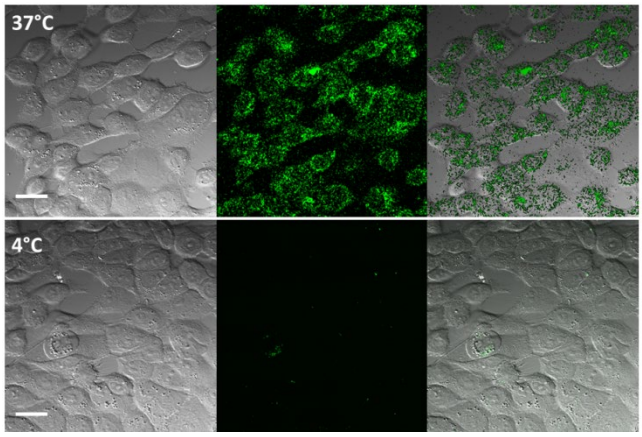

Fig. 5 Cell uptake mechanism study of the rhodamine-labeled B_{12}-Mn-1 at 37°C and 4°C using 16HBE14o- bronchial cells. Left: brightfield image, middle: rhodamine-labeled B_{12}-Mn-1 emission and right: overlay. The excitation wavelength was 480 nm and emission filter 550±10 nm. Scale bar: 20 μm.

2.4. Comparison of dark and light-induced cytotoxicity of photoCORMs

Having confirmed the cellular uptake of the derivatives, we studied the dark and light-induced cytotoxicity of the photoCORMs. First, the cytotoxicity of all 8 compounds was evaluated with the malignant cell line MCF-7. The cell viability upon treatment with free complexes Mn-**1** to -**4** was assessed using the MTT assay. As shown in Fig. 6, a dose-dependent killing of MCF-7 cells was observed in the dark. The experiments showed that Mn-**1** and -**4** have IC_{50} values below 10 μM (table 2). As expected, under the same conditions, the corresponding B_{12} photoCORMs display a general lower toxicity (Fig. 7). While B_{12}-Mn-**1** and -**4** are essentially nontoxic, B_{12}-Mn-**2** and -**3** are moderately toxic with IC_{50} values of 40 and 17 μM respectively after 48 hours of incubation. In a parallel experiment, the same cells were treated with the same compounds and irradiated with visible light (see ESI for details) after 24 hours of incubation. After photo-irradiation, the cells were incubated for another 24 hours before evaluating % survival. Interestingly, within experimental error, no obvious differences or trend could be discerned by comparing the toxicity values of the dark and light experiments.

As mentioned in the introduction, the complexity of the subject has led to the hypothesis that CO effects are highly cell-type dependent [4, 35, 48]. For this reason, we decided to repeat the experiments with two other human cancer cell lines; lung carcinoma A549 and colon adenocarcinoma HT29. The assays were repeated at high and low cell density. For these series of experiments only the compound B_{12}-Mn-**2** and its counterpart Mn-**2** were selected because of their moderate and

comparable activity against MCF-7. Once again, the % cell survival was compared under dark (no released CO) and light (released CO) conditions. Fig. 8 and 9 show respectively the results obtained by the MTT assay at low and high cell confluence.

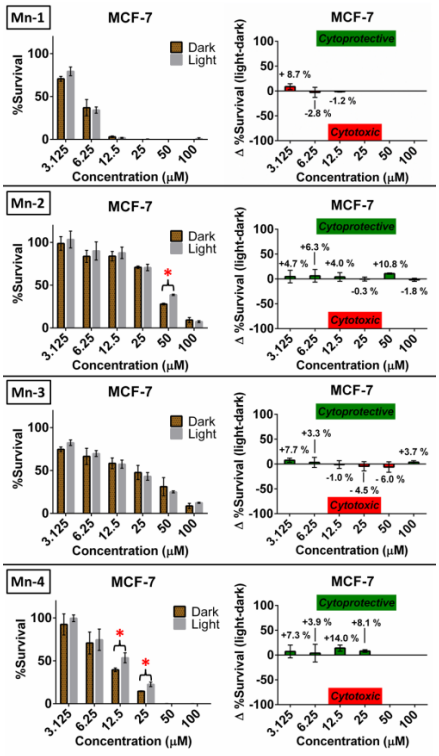

Fig. 6 Comparison of the dark and light cytotoxicity of the compounds Mn-**1** to -**4** against MCF-7 cell line. Left: experimental data, right: relative % of cancer cell survival of light vs dark conditions. Each experiment was done in triplicates, repeated three times (n=3) and data presented is the mean ± standard deviation (SD), *$p<0.05$.

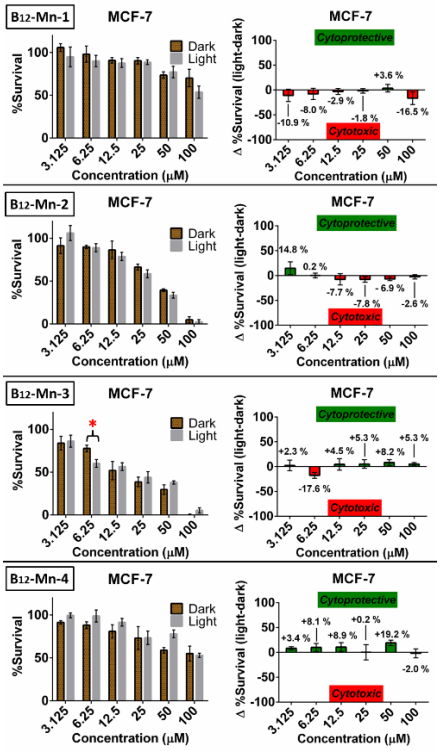

Fig. 7 Comparison of the dark and light cytotoxicity of the compounds B12-Mn-**1** to -**4** against MCF-7 cell line Left: experimental data, right: relative % of cancer cell survival of light vs dark conditions. Each experiment was done in triplicates, repeated three times (n=3) and data presented is the mean ± standard deviation (SD), *p<0.05.

Table 2. IC_{50} values (μM) of the compounds tested in this study against different cell lines under dark and photo-activated experimental conditions

Cell Line	*Compounds*	*Dark*	*Light*
MCF-7	**Mn-1**	4.4 ± 0.4	5.0 ± 0.2
	Mn-2	35.6 ± 5.1	36.2 ± 6.0
	Mn-3	15.1 ± 4.2	17.2 ± 2.1
	Mn-4	8.4 ± 2.2	12.6 ± 2.5
	B12-Mn-1	> 100	> 100
	B12-Mn-2	40.4 ± 4.3	30.2 ± 5.0
	B12-Mn-3	16.9 ± 4.4	17.4 ± 4.8
	B12-Mn-4	> 100	> 100
A549-LD	**Mn-2**	11.2 ± 1.9	11.9 ± 3.1
	B12-Mn-2	> 100	> 100
A549-HD	**Mn-2**	34.2 ± 7.3	25.6 ± 6.4
	B12-Mn-2	> 100	> 100
HT29-LD	**Mn-2**	11.3 ± 2.5	10.1 ± 2.2
	B12-Mn-2	82.04 ± 12.05	69.7 ± 14.6
HT29-HD	**Mn-2**	23.5 ± 7.1	28.3 ± 5.7
	B12-Mn-2	> 100	> 100
16HBE14o-	**Mn-2**	10.0 ± 2.4	14.6 ± 1.4
	B12-Mn-2	40.0 ± 8.3	> 100

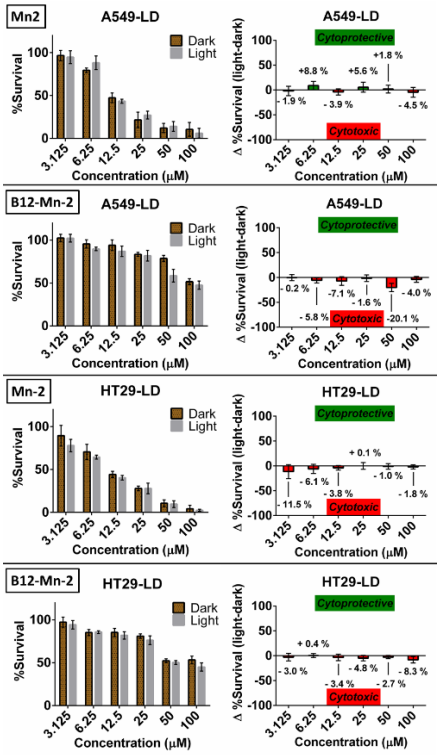

Fig. 8 Comparison of the dark and light cytotoxicity of the compounds B12-Mn-2 and Mn-2 against A549 and HT29 cell lines at low density (LD). Left: experimental data, right: relative % of cancer cell survival of light vs dark conditions. Each experiment was done in triplicates, repeated three times (n=3) and data presented is the mean ± standard deviation (SD).

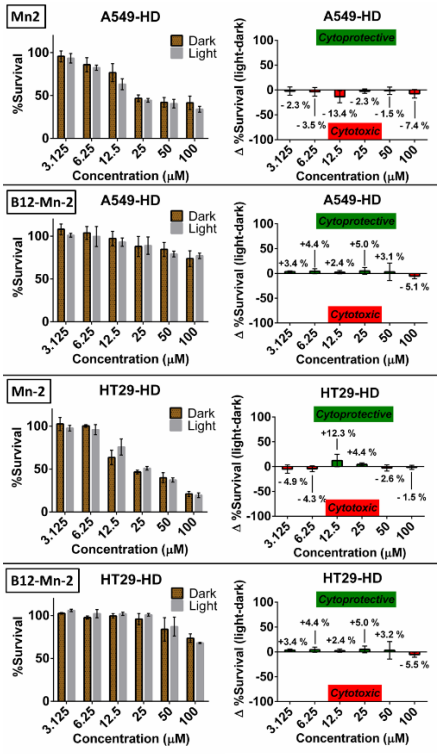

Fig. 9 Comparison of the dark and light cytotoxicity of the compounds B12-Mn-2 and Mn-2 against A549 and HT29 cell lines at high density. Left: experimental data, right: relative % of cancer cell survival of light vs dark conditions. Each experiment was done in triplicates, repeated three times (n=3) and data presented is the mean ± standard deviation (SD).

As it can be clearly appreciated from the graphs, the cytotoxicity of the relative compounds differs with respect to the cell density investigated (table 2). Higher cell confluence tends to decrease the effect of the complexes on the viability, which conversely, is more pronounced at low cell density. However, as observed with the MCF-7 cell line, a comparison of the relative % cell survival of dark and light experiment shows no trend and virtually no difference within experimental error.

At this stage of the study, we questioned the integrity of the photoCORMs as they were handled during the biological assays, because it is possible that sensitive photoCORMs could lose most of their CO in dilute solutions. Samples of Mn-**2** and B_{12}-Mn-**2** were therefore prepared in cell culture medium, exposed to experimental ambient lighting conditions and their solution stability monitored over the course of 24h. Analysis of the UV-visible spectra showed little or no change of the spectroscopic traces (ESI), indicating that the complexes did not degrade significantly during preparation of the biological assays (ca. 1h). We then investigated the ability of the photoCORMs to release CO after 24h incubation in the cell culture medium. The samples were, therefore, irradiated under experimental photolytic conditions and the results of the experiments are shown in Fig. 10. The spectroscopic changes are similar to the ones observed in standard solvents (see *CO-releasing properties of the compounds* section) and confirm that the CO releasing properties of the complexes are not compromised in the cell culture medium.

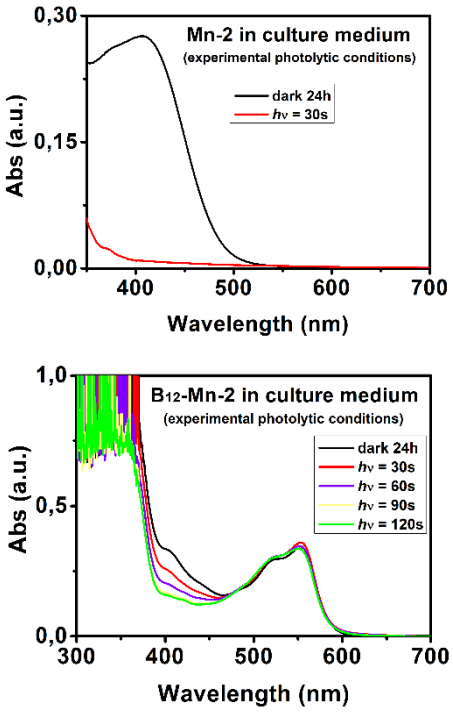

Fig. 10 Spectral changes in the electronic absorption spectrum of compounds Mn-**2** (top) and B_{12}-Mn-**2** incubated in cell culture medium for 24h and then irradiated with 420 nm light. The Mn-**2** complex was previously dissolved in DMSO (1% final concentration).

318 The unexpected observation related to the cytotoxicity of the complexes, prompted us to
319 perform other experiments in light of the fact that other established groups have reported eradication
320 of several types of cancer cells via delivery of CO from photoCORMs under illumination and that the
321 pro-apoptotic role of CO is now well established. First, the cytotoxicity of Mn-**2** and B_{12}-Mn-**2** was
322 evaluated against the CO-depleted complexes (i.e. inactive photoCORMs = i-photoCORMs,
323 comprising all photo-products including liberated ligands) according to the protocol described for
324 the previous experiments. i-photoCORMs were generated in solution by exposing them to visible
325 light for at least 30 min before cell treatment. In parallel experiments, the same cells were treated with
326 Mn-**2**, B_{12}-Mn-**2** and their corresponding i-photoCORMs. The complexes were then irradiated with
327 visible light after 24 hours of incubation and the cells viability was evaluated after an additional 24
328 hours of incubation (Fig. 11).
329 To our surprise i-photoCORMs displayed greater toxicity than the corresponding Mn-**2**, B_{12}-Mn-
330 **2** complexes in a concentration dependent manner. For i-photoCORM derived from Mn-**2** the greatest
331 effect is observed at a concentration of 12.5 μM. The relative difference in % of cancer cell survival
332 decreases at higher concentrations due to the inherent toxicity of Mn-**2** (see Fig. 6 and 7). i-
333 photoCORM derived from B_{12}-Mn-**2** shows more toxicity only at higher concentration (50 μM),
334 consistent with the fact that B_{12} conjugates are less toxic than their free complexes counterparts (Fig.
335 7 and Table 2). For B_{12}-Mn-**2**, at lower concentrations, comparison of the relative % cell survival shows
336 virtually no difference within experimental error (Fig. 11).
337

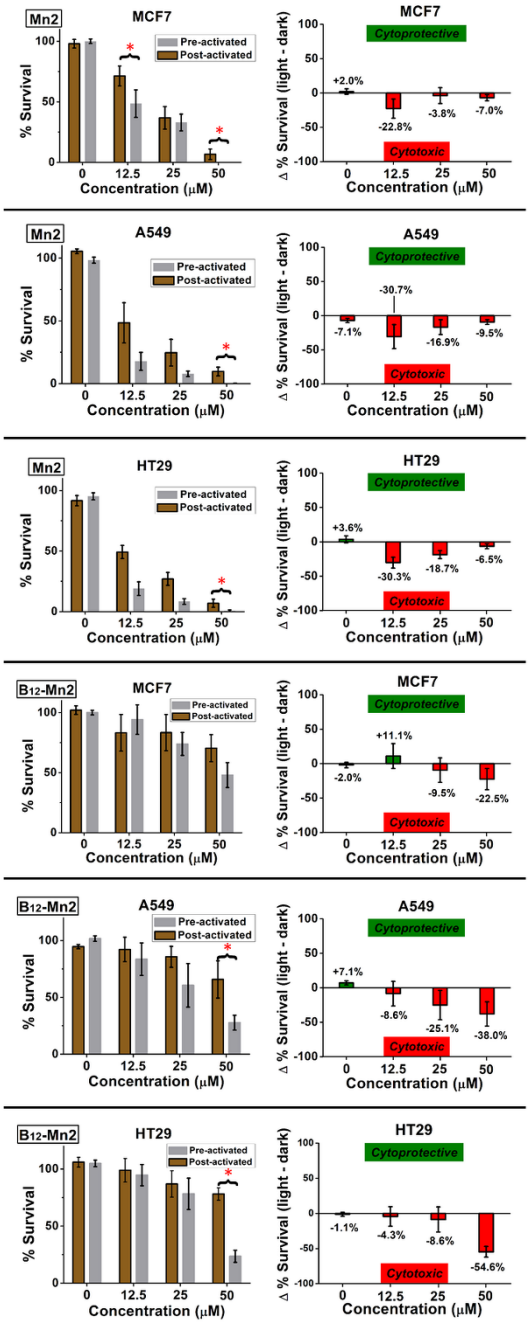

Fig. 11 Comparison of the cytotoxicity effects of the compounds Mn-**2** and B12-Mn-**2** (brown columns) and i-photoCORMs (gray columns) against different cell lines at low density (LD). Left: experimental data, right: relative % of cancer cell survival of light (i-photoCORMs) vs dark conditions (i.e. post-activated Mn-**2** or B12-Mn-**2**). Each experiment was done in triplicates, repeated three times (n=3) and data presented is the mean ± standard deviation (SD), *p<0.05.

The results of the experiments point to the possibility that for this specific set of photoCORMs bearing ethynyl-α-diimine ligands, the CO-depleted metal core and/or the released ligands are playing a fundamental role in their cytotoxicity and that the metal / ligand fragment is needed to maximize CO toxicity, and *vice versa*, both acting in concert. Different phenanthroline derivatives, e.g., are known to exert dose-dependent cytotoxic effects on different tumor cell lines [49-51]. To test

this hypothesis the cells were treated in parallel with Mn-**2**, B_{12}-Mn-**2** and i-photoCORMs in two different experiments. In one case, all species were irradiated at the onset of treatment (Fig. 12) and in the other all complexes were kept in the dark for the duration of treatment (Fig. 13). Cells viability was evaluated after 24 hours of incubation in both experiments. As it can be clearly appreciated from the graphs in Fig. 12, under conditions of immediate photolysis, the cytotoxicity of the relative compounds (i.e. Mn-**2** / B_{12}-Mn-**2** vs respective i-photoCORMs) shows virtually no difference within experimental error. If however, none of the complexes is irradiated (Fig. 13), the toxicity of Mn-**2** and B_{12}-Mn-**2** is drastically reduced (compare experimental data of Fig. 12 and 13). These results appear to confirm that the CO-depleted metal fragments are acting in combination with CO to determine the overall cytotoxicity of the species. HT29 cells, in particular, seem most sensitive to the action of the photo-products.

It should be noted at this point that, while the anticancer effects of photoCORMs bearing ethynyl-α-diimine ligands differ from other established photoCORMs, the observation we made in this study is not unprecedented. Until very recently, e.g., the role of CO in determining the antibacterial effectiveness of CORMs was never questioned; but new evidence has emerged for CORM-3. Antimicrobial studies on CORMs and photoCORMs generally indicate that the bactericidal effect of the molecules is due to CORM-derived CO leading to the hypothesis that CORMs act as CO-delivery systems capable of concentrating intracellularly their CO cargo. Carbon monoxide alone, however, is not as potent as CORMs and it does not elicit the same bactericidal effects as the molecules [52-54]. CO release alone in the medium cannot justify the antibacterial action of CORMs nor can the rate of CO liberation by CORMs explain the effects on bacteria growth [52-54]. Thus, it is clear that both CO and the metal fragment are important for the microbial toxicity of CORMs. To add complexity to the issue, studies have also reported that the antimicrobial effectiveness of CORMs can vary depending of the medium used for the *in vitro* experiments. In rich media or in the presence of molecules such as N-acetylcysteine, cysteine, reduced glutathione or other sulphur-rich species, the antimicrobial activity of CORMs (in particular CORM-3) is somewhat reduced (if not completely abrogated) against e.g. *E. coli* [52], *S. aureus* or *P. aeruginosa [55, 56]* but not against *S. Typhimurium* [57].

The role of thiols in rich media was not explained until recently in a study that demonstrated that active antimicrobial agent of CORM-3 is not CO but Ru^{2+}, which binds tightly to thiols [58]. Thus, thiols, amino acids and other sulphur-rich species in complex growth media protect bacteria against CORM-3 by binding and sequestering the metal ion. Additionally, in rich media after only 10 min following addition of CORM-3, less than 3% of the total CO ligands are biologically available [55, 59]. The study also showed a direct positive correlation between bacterial viability protection and amino

acid affinity for CORM-3 and compellingly demonstrated that the toxicity of the CORM cannot be attributed to CO release [58].

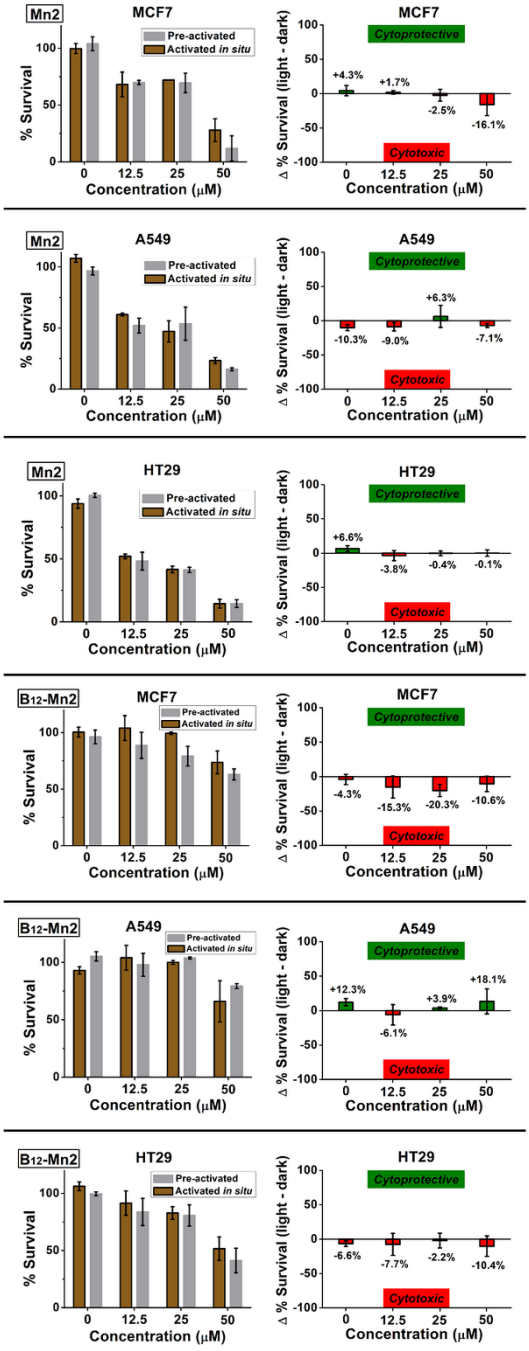

Fig. 12 Comparison of the cytotoxicity effects of the compounds Mn-**2** and B12-Mn-**2** (brown columns) and i-photoCORMs (gray columns) photo-activated at the onset of treatment, against different cell lines at low density (LD). Left: experimental data, right: relative % of cancer cell survival of light (i-photoCORMs) vs dark conditions (i.e. Mn-**2** or B12-Mn-**2** activated *in situ*). Each experiment was done in triplicates, repeated three times (n=3) and data presented is the mean ± standard deviation (SD), *$p<0.05$.

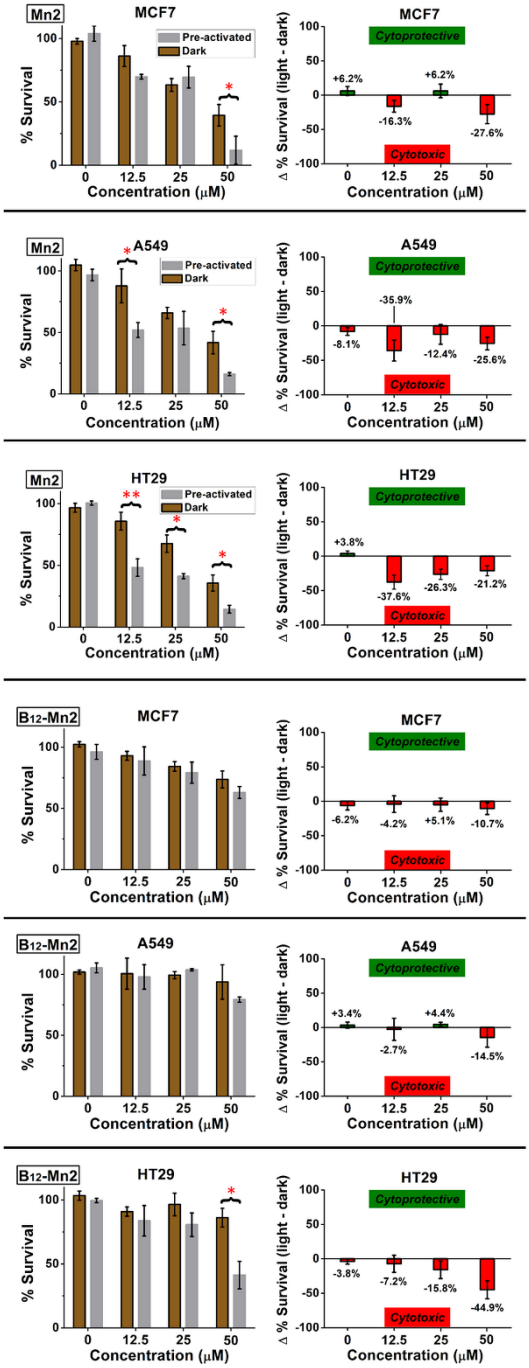

Fig. 13 Comparison of the dark cytotoxicity effects of the compounds Mn-**2** and B12-Mn-**2** (brown columns) and i-photoCORMs (gray columns) against different cell lines at low density (LD). Left: experimental data, right: relative % of cancer cell survival of light (i-photoCORMs) vs dark conditions (i.e. Mn-**2** or B12-Mn-**2**). Each experiment was done in triplicates, repeated three times (n=3) and data presented is the mean ± standard deviation (SD), *p<0.05, **p<0.01.

Finally, we decided to check the dark and light-induced effects of Mn-**2** and B12-Mn-**2** against 16HBE14o- cells, (SV-40 large T-antigen transformed bronchial epithelial cell line), and use it as a control. Typically, in such an experiment, it is expected that the dose of CO delivered will counterbalance the toxic effect of the complexes and thus display cytoprotective properties [4]. As

seen in the Fig. 14, this result is clearly observed with both compounds and confirms the cytoprotective activity of CO derived from these photoCORMs. A closer look also reveals that for the B_{12} derivatives, the effect seems to reach a plateau. Indeed, normal cells will saturate in cobalamin thus preventing intracellular accumulation of the vitamin beyond a certain threshold. Regarding the Mn-**2** complex, the cytoprotective effect is also demonstrated at lower concentration, but is attenuated gradually as the concentration increases. As it seems, the fact that Mn-**2** can passively cross the cell membrane is contributing to this reversed trend. In this case, the intrinsic toxicity of Mn-**2** and the release of about three equivalents of CO seem to generate synergistic deleterious effects. We finally note in passing that by conducting LDH assays, we were able to determine that cells death was not following a necrotic pathway under dark or light conditions (ESI).

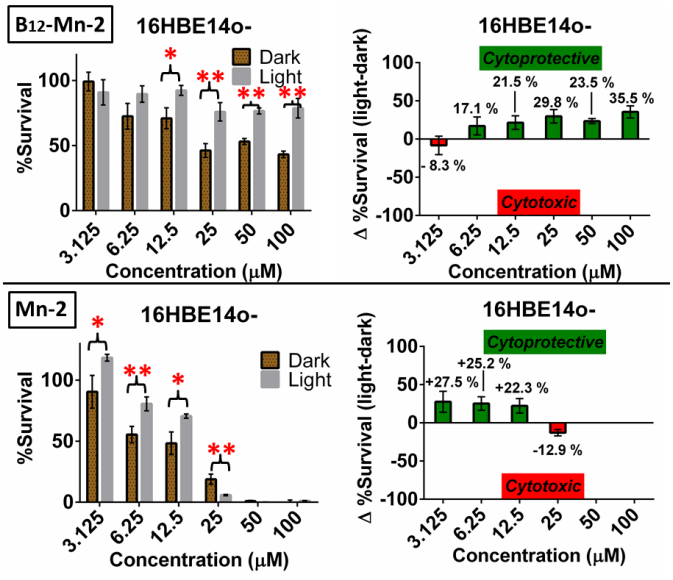

Fig. 14 Comparison of the dark and light cytotoxicity of the compounds B_{12}-Mn-2 and Mn-2 against 16HBE14o- cell line. Left: experimental data, right: relative % of cancer cell survival of light vs dark conditions. Each experiment was done in triplicates, repeated three times (n=3) and data presented is the mean ± standard deviation (SD), *p<0.05, **p<0.01.

4. Conclusions

In summary, we have reported the synthesis a series of photoCORM complexes of the well-known fac-$[Mn(CO)_3]^+$ core and ethynyl-α-diimine ligands, their cobalamin conjugates and their toxicity against the MCF-7, A549 and HT29 cancer cell lines. The present investigation was stimulated by our observation of the unusual dark and light-induced cytotoxicity of the complexes, which had appeared to us as not being directly related to their released CO. However, our results indicate that both CO and CO-depleted metal fragments (i.e. photo-products including ligands) play a role in the cytotoxicity of these Mn-based photoCORMs. It is unclear to us at the present stage why or how the ethynyl-α-diimine ligands influence the anticancer activity of the molecules and render the CO-

depleted metal fragments of Mn-**2** and B_{12}-Mn-**2** active. We have previously shown that, e.g., NO release of organic N-nitrosamine is activated if the molecules are in contact with cultured cells [60]. Here perhaps a similar slow activation is at play for these photoCORMs. As suggested for other species [61], the molecules may thus possess a 'Janus-headed' activity, whereby the metal complexes deliver and concentrate CO to cells, while at the same time, the CO ligands mask the metal-ligand fragment from its mode of action (i.e. acting as photolabile 'protective groups' for the metal and/or ligand fragment). Finally, we emphasize that the results and observations reported in this study should not be generalized for other Mn-based photoCORMs. The vast majority of these molecules bear benign ligands to determine the exact effects of CO on the process of cell death.

5. Materials and Methods

5.1. General experimental details

All chemicals were purchased from Sigma-Aldrich (St Louis, MO) and used without further purification. The compounds Mn-**1** to -**4** were dissolved in DMSO (0.1% final volume) and diluted in their respective media prior to their use in biological experiments while the compounds B_{12}-Mn-**1** to -**4** were only dissolved in the medium. Human breast adenocarcinoma MCF-7 cells were obtained from the Department of Medicine at the University of Fribourg (Switzerland). Human lung carcinoma A549 and human colon colorectal adenocarcinoma HT29 were purchased by ATCC while immortalized human bronchial epithelial cells 16HBE14o- were kindly given by Dr. Gruenert (University of California, San Francisco). The MCF-7 and HT29 cells were maintained in Dulbecco's Modified Eagle's Medium supplemented with 10% Fetal bovine serum (FBS), 1% L-Glutamine and 1% Penicilin/Streptavidin (cDMEM). The A549 cells were maintained in Roswell Park Memorial Institute Medium supplemented with 10% Fetal bovine serum (FBS), 1% L-Glutamine and 1% Penicilin/Streptavidin (cRPMI) and 16HBE14o- cells in Minimum Essential Medium supplemented with 10% Fetal bovine serum (FBS), 1% L-Glutamine and 1% Penicilin/Streptavidin (cMEM) (all media and supplements were purchased from Gibco) at 37 °C with 5% CO_2. Additionally, cell culture media for MCF-7 was supplemented with 10 $\mu g*mL^{-1}$ human recombinant insulin (Gibco) and cell culture media for HT29 supplemented with 1x NEAA (non-essential amino acids, Gibco). The sensitive adherent 16HBE14o- cells were cultured using coated flaks (Cell+ growth surface for sensitive adherent cells, Sarstedt, item N° 83.3911.302). The cells were cultured in their respective medium and split until resuming exponential growth. Subsequently, the cells were seeded in 96-well plates at a density of 2×10^3 cells per well. Prior to the seeding of 16HBE14o- cells, a fibronectin/collagen coating was applied to the 96 well plates as previously described [62]. The cells were grown for either 1 (MCF-7, 16HBE14o-, A549 and HT29) or 5 days (A549 and HT29). Then, the media were removed, and the cells treated with Mn-**1** to -**4** and B_{12}-Mn-**1** to -**4** (conc. of 100, 50, 25,

12.5, 6.25, 3.25 μM, 200 μl per well, in triplicate), in separated 96 well plates in order to perform dark and light experiment. The light exposure was performed after 24 hours, as previously reported [31], by exposing the cells to a 10W power white LED placed at approximately 20 cm of the plate surface for 90 seconds (an amount of time which was determined to release all the CO ligands from the compounds under the myoglobin assay conditions performed at several position in the 96 well plates). In parallel, another batch was kept in the dark for the whole 48 hours of the drugs exposure. As a positive control, 0.2% Triton X in medium was systematically used. The light exposures of the cells were performed using a commercial white led (10W, Ayca) while the myoglobin assays were done in a UV-Vis cuvette with an Atlas Photonics LUMOS 43 as a 420 nm light source. The preparative separations of the B_{12} derivatives were conducted on a Macherey–Nagel Nucleodur C18 HTec column (5 μm particle size, 110 Å pore size, 250 × 21 mm). HPLC solvents were aqueous trifluoroacetic acid 0.1% (A) and methanol (B). The compounds were separated using the following gradient: 0–5 min (75% solvent A), 5–35 (75% solvent A → 0% solvent A), 35–45 min (100% solvent B). The flow rate was set to 5 ml*min^{-1} for the preparative separation. The eluting bands were detected at 320 nm. IR spectra were measured using a Perkin Elmer FTIR Frontier Serie 99155 equipped with a PIKE TECHNOLOGIES GladiATRTM system. High resolution ESI-MS was performed on a Bruker FTMS 4.7-T Apex II and the measurements were recorded in the positive mode while routine mass analysis were recorded on a Bruker Esquire HCT. NMR analyses were recorded on a Bruker Avance III 500 MHz. The corresponding ^{1}H and ^{13}C chemical shifts are reported relative to residual solvent protons and carbons. The UV-Vis spectra were recorded on a Jasco V-730. X-ray data collections were measured at low temperature using CuK_{α} radiation on a Rigaku SuperNova dual system in combination with an Atlas CCD detector. Measurements of the formazan products were done using a microplate reader Hidex 425-301. Live cell imaging was performed using a laser confocal scanning microscope (cLSM 710, Carl Zeiss, Göttingen, Germany) with a 63× oil-immersion objective lens and equipped with an incubation chamber providing controlled temperature of 37°C, moisture and CO_2 atmosphere. The 50% confluent 16HBE14o- cells were incubated in cover glass bottom cell chamber slides (Nunc Lab-Tek, 1.7 cm^2 per well) with B_{12}-Mn-**1**-CBC for 30 min at 4°C and at 37°C in parallel. Subsequently, the media was removed, the chambers washed three times with PBS and viewed under the microscope with an excitation wavelength of 480 nm and a detection range of 550 ± 10 nm. These conditions did not produce any background fluorescence in the control cells. The emission pictures represented in the figure 5 were modified equally in brightness, contrast and noise removal to aid the visualization only with the software ImageJ.

499 *5.2. Cytotoxicity assay*

500 The IC_{50} values were determined using the cell lines MCF-7, HT29, A549 and 16HBE14o-.
501 Subsequently, the medium was collected for lactate dehydrogenase (LDH) assay, and the wells
502 refilled with fresh solution of 200 µl of 10x diluted MTT stock solution (5 $mg*ml^{-1}$). The plates were
503 then incubated for 4 hours at 37 °C. After removal of the media, 100 µl of DMSO were added to each
504 well and the plates re-incubated at 37 °C for another 15 minutes and then shaken for 10 minutes. The
505 absorbance's were measured using Hidex 425-301 microplate reader at 560 nm (MTT assay). The
506 amount of LDH released into each well was evaluated following manufacturer's protocol (Roche,
507 Switzerland, N° 11644793001). Finally, the reading was performed using microplate reader at 490 nm
508 using the 630 nm filter (for LDH). The IC50 values as well as the statistical significant t-test were
509 calculated using Graphpad Prism 6 and red asterisks (*) were used to report the significant
510 differences on the graphs between the dark and light experiments for *$p>0.05$ and **$p<0.01$.

511 *5.3. Compounds and Ligands synthesis*

512 The ligands 4'-ethynyl-2,2'-bipyridine (**L1**) and 5-ethynyl-1,10-phenanthroline (**L2**) were prepared as
513 previously reported [63, 64].

514 5-ethynyl-2,9-dimethyl-1,10-phenanthroline (**L3**): To 5-bromo-2,9-dimethyl-1,10-phenanthroline
515 (200 mg, 0.70 mmol, 1 eq.) were successively added $[PdCl_2(PPh_3)_2]$ (14,8 mg, 0.021 mmol, 3 mol%),
516 copper iodide (13.3 mg, 0.070 mmol, 10 mol%), argon-degassed dry THF (10.0 mL), diisopropylamine
517 (2.4 mL, 1.76 g, 17.5 mmol, 25 eq.) and (trimethylsilyl)acetylene (0.14 mL, 92.3 mg, 1.05 mmol, 1.5 eq.)
518 under an argon atmosphere. The reaction mixture was stirred at room temperature overnight, then
519 heated at reflux for 3 hours. The reaction mixture was filtered through a silica plug and the silica
520 washed with THF and Et_2O. After removal of the solvents under reduced pressure, the brown oil was
521 then dissolved in CH_3OH and treated with K_2CO_3 (116 mg, 0.84 mmol, 1.2 eq.). The complete TMS-
522 alkynyl deprotection was achieved after stirring 4 hours at room temperature. The reaction was then
523 quenched with water and the organic solvent evaporated under vacuum. The residue was extracted
524 with CH_2Cl_2 (3 x 30 mL), and the organic layers washed with brine and dried over $MgSO_4$. The crude
525 product was purified by flash column chromatography (silica gel, CH_2Cl_2/CH_3OH 98:2) to yield 93
526 mg (0.73 mmol, 65%) of 5-ethynyl-2,9-dimethyl-1,10-phenanthroline (**L3**) as a beige solid. **^{1}H NMR**
527 (500 MHz, $CDCl_3$-[d1]): δ = 8.69 (d, J = 8.4 Hz, 1H), 8.15 (d, J = 8.24 Hz, 1H) 8.02 (s, 1H), 7.62 (d, J = 8.4
528 Hz, 1H), 7.55 (d, J = 8.25 Hz, 1H), 3.52 (s, 1H), 2.98 (s, 3H), 2.97 (s, 3H) ppm; **HR-ESI-MS** (ESI^+): $[M+H]^+$
529 = 233.1074, calculated for $C_{16}H_{13}N_2$ = 233.1073.
530
531 4'-ethynyl-6,6'-dimethyl-2,2'-bipyridine (**L4**): To 4'-bromo-6,6'-dimethyl-2,2'-bipyridine [65]
532 (200 mg, 0.76 mmol, 1 eq.) were successively added $[PdCl_2(PPh_3)_2]$ (16,3mg, 0.023 mmol, 3 mol%),

copper iodide (14.5 mg, 0.076 mmol, 10 mol%), argon-degassed dry THF (10.0 mL), diisopropylamine (2.6 mL, 1.92 g, 19 mmol, 25 eq.) and (trimethylsilyl)acetylene (0.15 mL, 100 mg, 1.14 mmol, 1.5 eq.) under an argon atmosphere. The reaction mixture was stirred at room temperature overnight, then heated at reflux for 3 hours. The reaction mixture was filtered through a silica plug and the silica washed with THF and Et_2O. After removal of the solvents under reduced pressure, the brown oil was then dissolved in CH_3OH and treated with K_2CO_3 (126 mg, 0.91 mmol, 1.2 eq.). The complete TMS-alkynyl deprotection was achieved after stirring 4 hours at room temperature. The reaction was then quenched with water and the organic solvent evaporated under vacuum. The residue was extracted with CH_2Cl_2 (3 x 30 mL), and the organic layers washed with brine and dried over $MgSO_4$. The crude product was purified by flash column chromatography (silica gel, CH_2Cl_2/CH_3OH 99:1) to yield 109 mg (0.52 mmol, 69%) of 4'-ethynyl-6,6'-dimethyl-2,2'-bipyridine (**L4**) as a beige solid. **^{1}H NMR** (500 MHz, $CDCl_3$-[d1]): δ = 8.28 (br s, 1H), 8.17 (d, J = 7.8 Hz, 1H) 7.68 (t, J = 7.8 Hz, 1H), 7.22 (br s, 1H), 7.16 (d, J = 7.7 Hz, 1H), 3.25 (s, 1H), 2.63 (s, 3H), 2.62 (s, 3H) ppm; **HR-ESI-MS** (ESI^+): $[M+Na]^+$ = 231.0887, calculated for $C_{14}H_{12}N_2Na$ = 231.0892.

Bromopentacarbonylmanganese(I) (150 mg, 0.55 mmol, 1 eq.) and the respective alkynes (**L1, L2, L3** or **L4**, 1.1 eq.) were stirred in THF (20 ml) under dark conditions. After 4 hours, hexane (80 ml) was added to the mixtures and bright yellow precipitates formed in each case. The solids were isolated by vacuum filtration and washed with hexane (50 ml). Crystals were obtained by layering hexanes over solutions of the complexes in dichloromethane.

Mn-**1** (complex $[MnBr(CO)_3(HCC\text{-}bpy)]$): Yield 186.5 mg (85%). **^{1}H NMR** (500 MHz, $CDCl_3$-[d1]): δ = 9.22 (d, J = 5.0 Hz, 1H), 9.18 (d, J = 5.6 Hz, 1H) 8.18 (s, 1H), 8.15 (d, J = 8.0 Hz, 1H), 8.00 (t, J = 7.6 Hz, 1H), 7.60-7.52 (m, 2H), 3.65 (s, 1H) ppm; **^{13}C NMR** (125 MHz, $CDCl_3$-[d1]): δ= 155.4, 154.6, 153.4, 153.1, 138.3, 132.6, 127.9, 126.3, 124.4, 122.2, 85.5, 79.0 ppm; **UV/Vis** spectrum in methanol solution: λ_{max} (Ɛ, $Lmol^{-1}cm^{-1}$) = 415 (2350); **IR** (ATR, cm-1): νC≡C = 2109, νC≡O = 2020, 1913, 1887.

Mn-**2** (complex $[MnBr(CO)_3(HCC\text{-}phen)]$): Yield 186.1 mg (80%). **^{1}H NMR** (500 MHz, $CDCl_3$-[d1]): δ = 9.58 (d, J = 5.1 Hz, 1H), 9.54 (d, J = 5.1 Hz, 1H) 8.91 (d, J = 8.4 Hz, 1H), 8.47 (d, J = 8.4 Hz, 1H), 8.24 (s, 1H), 7.96 (dd, J = 8.4, 5.1 Hz, 2H), 7.88 (dd, J = 8.4, 5.1 Hz, 1H), 3.75 (s, 1H) ppm; **^{13}C NMR** (125 MHz, $CDCl_3$-[d1]): δ= 153.9, 153.8, 146.7, 146.6, 136.9, 135.9, 131.7, 130.0, 129.1, 125.5(7), 125.5(5), 121.2, 85.3, 78.2 ppm, **UV/Vis** spectrum in methanol solution: λ_{max} (Ɛ, $Lmol^{-1}cm^{-1}$) = 408 (2933); **IR** (ATR, cm-1): νC≡C = 2107, νC≡O = 2020, 1938, 1906.

Mn-**3** (complex $[MnBr(CO)_3(HCC\text{-}phenMe_2)]$): Yield 193.5 mg (78%). **^{1}H NMR** (500 MHz, $CDCl_3$-[d1]): δ = 8.75 (d, J = 8.4 Hz, 1H), 8.27 (d, J = 8.30 Hz, 1H) 8.08 (s, 1H), 7.77 (d, J = 8.4 Hz, 1H), 7.70 (d, J = 8.3 Hz, 1H), 3.67 (s, 1H), 3.37 (s, 3H), 3.36 (s, 3H) ppm; **^{13}C NMR** (125 MHz, $CDCl_3$-[d1]): δ= 164.7, 164.3, 148.1, 147.9, 136.8, 135.6, 130.4, 127.7, 127.0, 126.2, 126.0, 118.3, 84.1, 78.4, 29.1(5), 29.1(1) ppm.

UV/Vis spectrum in methanol solution: λ_{max} (Ɛ, $Lmol^{-1}cm^{-1}$) = 388 (2295); **IR** (ATR, cm-1): νC≡C = 2111, νC≡O = 2019, 1940, 1909.

Mn-**4** (complex [$MnBr(CO)_3(HCC\text{-}bpyMe_2)$]): Yield 193.0 mg (82%).**^{1}H NMR** (500 MHz, $CDCl_3$-[d1]): δ = 7.95 (br s, 1H), 7.94 (d, J = 8.6 Hz, 1H) 7.85 (t, J = 7.8 Hz, 1H), 7.41 (br s, 1H), 7.40 (d, J = 7.5 Hz, 1H), 3.50 (s, 1H), 3.19 (s, 3H), 3.17 (s, 3H) ppm; **^{13}C NMR** (125 MHz, $CDCl_3$-[d1]): δ= 162.6, 162.4, 157.4, 156.7, 137.1, 131.7, 126.9, 125.3, 121.1, 118.9, 84.0, 78.7, 27.7, 27.5 ppm. **UV/Vis** spectrum in methanol solution: λ_{max} (Ɛ, $Lmol^{-1}cm^{-1}$) = 395 (3865); **IR** (ATR, cm-1): νC≡C = 2109, νC≡O = 2013, 1914, 1877.

5.4. General synthesis of the vitamin B12 derivatives

The following procedure was adapted from the literature to achieve the synthesis of the B_{12} derivatives [40]. A mixture of cyanocobalamin (20 mg, 0.014 mmol, 1 eq.), CuAcO (2.3 mg, 0.002 mmol, 0.1 eq.) and the respective alkynes (Mn-**1**, Mn-**2**, Mn-**3** and Mn-**4**, 5 eq.) were stirred in DMA (3.5 ml) until dissolution. Then, DBU (0.01 ml, 0.07 mmol, 5 eq.) was added and the solutions allowed to react at room temperature for 4 hours. The respective crudes were precipitated by dropwise addition to stirred solutions of diethyl ether/CH_2Cl_2 (50 ml, 1:1). After filtration, the residues were dissolved in a mixture of CH_3OH and water (2 ml, 1:1), filtered again and purified by preparative HPLC. The eluting bands containing the desired products were isolated and lyophilized.

B_{12}-Mn-**1**: Yield 21.7 mg (85%). **^{1}H NMR** (500 MHz, D_2O-[d1]): δ = 9.26 (d, J = 5.5 Hz, 1H), 8.97 (d, J = 5.8 Hz, 1H), 8.25-8.17 (m, 2H), 8.13 (d, J = 8.2 Hz, 1H), 7.75-7.67 (m, 2H), 7.3 (s, 1H), 7.19 (s, 1H), 7.16-7.11 (m, 1H), 6.58 (s, 1H), 6.38 (d, J = 3.2 Hz, 1H), 6.09 (s, 1H), 4.38-4.28 (m, 2H), 4.15-4.07 (m, 1H), 3.96 (dd, J = 13.0, 2.35 Hz, 1H), 3.79 (dd, J = 13.0, 3.9 Hz, 1H), 3.68-3.57 (m, 1H), 3,46 (dd, J = 11.8, 5.0 Hz, 1H), 3.32 (d, J = 10 Hz, 1H), 3.06-2.96 (m, 1H), 2.82-2.40 (m, 20H), 2.29 (s, 6H), 2.16 (d, J = 13.0 Hz, 2H), 2.10-1.94 (m, 6H), 1.92-1.79 (m, 5H), 1.47 (s, 3H), 1.42 (s, 3H), 1.39 (s, 3H), 1.28 (d, J = 6.3 Hz, 3H), 1.21 (s, 3H), 1.16-1.01) (m, 2H), 0.53 (s, 3H) ppm; **UV/Vis** spectrum in methanol solution: λ_{max} (Ɛ, $Lmol^{-1}cm^{-1}$) = 366 (13020), 401 (5326), 527 (4858), 551 (5420); **IR** (ATR, cm-1): νC≡C = 2026, νC≡O = 2035, 1937, 1924; **HR-ESI-MS** (ESI^+): $[M\text{-}Br+H]^{2+}$ = 823.7780, calculated for $C_{77}H_{96}Co_1Mn_1N_{15}O_{17}P_1$ = 823.7774.

B_{12}-Mn-**2**: Yield 20.5 mg (80%). **^{1}H NMR** (500 MHz, D_2O-[d1]): δ = 9.64-9.56 (m, 1H), 9.50 (d, J = 5.0 Hz, 1H), 8.55 (d, J = 8.4 Hz, 1H), 8.02 (dd, J = 8.6, 5.25 Hz, 1H), 7.96 (ddd, J = 8.4, 5.25, 1.45 Hz, 1H), 7.78 (d, J = 1.63 Hz, 1H), 7.31 (s, 1H), 7.22 (s, 1H), 6.61 (s, 1H), 6.39 (d, J = 3.1 Hz, 1H), 6.11 (s, 1H), 4.47-4.26 (m, 4H), 4.16-4.09 (m, 1H), 3.97 (d, J = 13.0 Hz, 1H), 3.80 (dd, J = 13.0, 3.7 Hz, 1H), 3.63 (d, J = 14.3 Hz, 1H), 3.50-3.42 (m, 1H), 3.38 (d, J = 9.40 Hz, 1H), 3.00 (dd, J = 14.7, 5.40 Hz, 1H), 2.83-2.72 (m, 1H), 2.72-2.46 (m, 16H), 2.44-2.37 (m, 3H), 2.29 (s, 6H), 2.26-2.14 (m, 2H), 2.14-1.94 (m, 7H), 1.90-1.76 (m, 5H), 1.48 (s, 3H), 1.40 (s, 3H), 1.29 (d, J = 4.17 Hz, 3H), 1.27 (d, J = 6.40 Hz, 3H), 1.21 (d, J = 3.6 Hz, 3H),

1.17-1.04 (m, 3H), 0.54 (s, 3H) ppm; **UV/Vis** spectrum in methanol solution: λ_{max} (Ɛ, $Lmol^{-1}cm^{-1}$) = 401 (6328), 528 (5268), 551 (5789); **IR** (ATR, cm-1): νC≡C = 2119, νC≡O = 2042, 1946, 1944; **HR-ESI-MS** (ESI^+): $[M-Br+Na+H]^{2+}$ = 846.7683, calculated for $C_{79}H_{95}Co_1Mn_1N_{15}O_{17}P_1Na_1$ = 846.7683.

B_{12}-Mn-**3**: Yield 13.0 mg (50%). **^{1}H NMR** (500 MHz, $CDCl_3$-[d1]): δ = 8.29-8.15 (m, 1H), 8.11-8.01 (m, 1H), 7.87-7.74 (m, 1H), 7.46 (d, J = 2.0 Hz, 1H), 7.36-7.24 (m, 2H), 7.20 (d, J = 3.75, 1H), 6.59 (d, J = 3.55 Hz, 1H), 6.39 (d, J = 2.60 Hz, 1H), 6.14-6.05 (m, 1H), 4.49-4.24 (m, 4H), 4.16-4.08 (m, 1H), 4.00-3.92 (m, 1H), 3.84-3.75 (m, 1H), 3.62 (d, J = 14.3 Hz, 1H9, 3.49-3.40 (m, 1H), 3.36 (d, J = 8.7 Hz, 1H), 3.30-3.15 (m, 4H), 3.10-2.88 (m, 5H), 2.86-2.44 (m, 19H), 2.44-2.23 (m, 10H), 2.22-1.68 (m, 16H), 1.47 (d, J = 19.4 Hz, 3H), 1.42-1.36 (m, 5H), 1.39 (d, J = 3.35 Hz, 3H), 1.37 (s, 2H), 1.29-1.24 (m, 5H), 1.19 (d, J = 5.9 Hz, 3H), 1.14-1.00 (m, 3H), 0.53 (br s, 3H) ppm; **UV/Vis** spectrum in methanol solution: λ_{max} (Ɛ, $Lmol^{-1}cm^{-1}$) = 401 (4009), 529 (3895), 550 (4188); **IR** (ATR, cm-1): νC≡C = 2122, νC≡O = 2030, 1930, 1923; **HR-ESI-MS** (ESI^+): $[M-Br+H]^{2+}$ = 849.7938, calculated for $C_{81}H_{100}Co_1Mn_1N_{15}O_{17}P_1$ = 849.7930.

B_{12}-Mn-**4**: Yield 19.4 mg (75%).**^{1}H NMR** (500 MHz, $CDCl_3$-[d1]): δ = 7.87 (sextet, d = 4.0 Hz, 1H), 7.68 (t, J = 6.6 Hz, 1H), 7.35-7.25 (m, 2H), 7.21 (s, 1H), 7.08 (d, J = 4.4 Hz, 1H), 6.69 (s, 0.5 H), 6.47 (s, 0.5 Hz), 6.45 (s, 1H), 6.30 (s, 1H), 6.0 (d, J = 5.6 Hz, 1H), 4.30-4.16 (m, 4H), 4.06-3.99 (m, 1H), 3.87 (d, J = 12.3 Hz, 1H), 3.70 (dd, J = 12.6, 3.9 Hz, 1H), 3.54 (d, J = 14.4 Hz, 1H), 3.49-3.38 (m, 1H), 3.20 (d, J = 9.2 Hz, 1H), 2.97-2.82 (m, 4H), 2.72-2.24 (m, 23H), 2.22-2.15 (m, 7H), 2.14-1.84 (m, 8H), 1.84-1.65 (m, 5H), 1.43 (s, 2H), 1.40 (s, 1H), 1.38 (s, 2H), 1.34-1.26 (m, 4H), 1.19 (d, J = 6.2 Hz, 3H), 1.14 (d, J = 9 Hz, 3H), 0.52 (br s, 3H) ppm; **UV/Vis** spectrum in methanol solution: λ_{max} (Ɛ, $Lmol^{-1}cm^{-1}$) = 366 (10565), 528 (4223), 551 (4717); **IR** (ATR, cm-1): νC≡C = 2120, νC≡O = 2036, 1943, 1939; **HR-ESI-MS** (ESI^+): $[M-Br+H]^{2+}$ = 837.7934, calculated for $C_{79}H_{100}Co_1Mn_1N_{15}O_{17}P_1$ = 837.7930.

B_{12}-Mn-**2**-CBC: An amount of 5 mg of CBC (rhodamine-labeled cyanocobalamin) was used as a starting material.[5] Yield 2.5 mg (42%). **MS** (ESI^+): $[M-Br+3H]^{3+}$ = 786.6 calculated for $C_{117}H_{144}Co_1Mn_1N_{19}O_{25}P_1$ = 786.6.

Author Contributions: F.Z. designed and coordinated the overall experimental program with the help of B.R-.R. J.R. synthesized and characterized the complexes. J. R. and J. D. studied their solution chemistry and spectroscopy. L.H. designed and carried out the *in vitro* studies. D. H. carried out the laser scanning microcopy experiments. J.D. and F.Z. wrote the manuscript, and all authors contributed to the final version.

Funding: Financial support from the Swiss National Science Foundation (Grant# PP00P2_170589) is gratefully acknowledged. L. H., D. H. and B. R. R. acknowledge the support by the Swiss National Science Foundation through the National Centre of Competence in Research "Bio-Inspired Materials" and the Adolphe Merkle Foundation.

Acknowledgments: We thank Dr. Gruenert (University of California, San Francisco) for providing the 16HBE14o- cell line.

Conflicts of Interest: The authors declare no conflict of interest.

References

[1] M.D. Maines, FASEB J, vol. 2, 1988, pp. 2557-2568.

[2] L. Wu, R. Wang, Pharmacol. Rev., vol. 57, 2005, pp. 585-630.

[3] R. Motterlini, L.E. Otterbein, Nat. Rev. Drug Discov., vol. 9, 2010, pp. 728-743.

[4] C. Szabo, Nat. Rev. Drug Discov., vol. 15, 2016, pp. 185-203.

[5] H. Was, J. Dulak, A. Jozkowicz, Curr. Drug Targets, vol. 11, 2010, pp. 1551-1570.

[6] P.O. Berberat, Z. Dambrauskas, A. Gulbinas, T. Giese, N. Giese, B. Kunzli, F. Autschbach, S. Meuer, M.W. Buchler, H. Friess, Clin. Cancer Res., vol. 11, 2005, pp. 3790-3798.

[7] G. Sass, P. Leukel, V. Schmitz, E. Raskopf, M. Ocker, D. Neureiter, M. Meissnitzer, E. Tasika, A. Tannapfel, G. Tiegs, Int. J. Cancer, vol. 123, 2008, pp. 1269-1277.

[8] M.A. Alaoui-Jamali, T.A. Bismar, A. Gupta, W.A. Szarek, J. Su, W. Song, Y. Xu, B. Xu, G. Liu, J.Z. Vlahakis, G. Roman, J. Jiao, H.M. Schipper, Cancer Res., vol. 69, 2009, pp. 8017-8024.

[9] J. Fang, T. Sawa, T. Akaike, T. Akuta, S.K. Sahoo, G. Khaled, A. Hamada, H. Maeda, Cancer Res., vol. 63, 2003, pp. 3567-3574.

[10] S.K. Sahoo, T. Sawa, J. Fang, S. Tanaka, Y. Miyamoto, T. Akaike, H. Maeda, Bioconjug. Chem., vol. 13, 2002, pp. 1031-1038.

[11] A. Kappas, G.S. Drummond, T. Manola, S. Petmezaki, T. Valaes, Pediatrics, vol. 81, 1988, pp. 485-497.

[12] A. Kappas, G.S. Drummond, C. Henschke, T. Valaes, Pediatrics, vol. 95, 1995, pp. 468-474.

[13] S.B. Dover, M.R. Moore, E.J. Fitzsimmons, A. Graham, K.E. McColl, Gastroenterology, vol. 105, 1993, pp. 500-506.

[14] G. Gueron, A. De Siervi, M. Ferrando, M. Salierno, P. De Luca, B. Elguero, R. Meiss, N. Navone, E.S. Vazquez, Mol. Cancer Res., vol. 7, 2009, pp. 1745-1755.

[15] C. Zou, H. Zhang, Q. Li, H. Xiao, L. Yu, S. Ke, L. Zhou, W. Liu, W. Wang, H. Huang, N. Ma, Q. Liu, X. Wang, W. Zhao, H. Zhou, X. Gao, Carcinogenesis, vol. 32, 2011, pp. 1840-1848.

[16] B. Wegiel, D. Gallo, E. Csizmadia, C. Harris, J. Belcher, G.M. Vercellotti, N. Penacho, P. Seth, V. Sukhatme, A. Ahmed, P.P. Pandolfi, L. Helczynski, A. Bjartell, J.L. Persson, L.E. Otterbein, Cancer Res., vol. 73, 2013, pp. 7009-7021.

[17] L. Vitek, H. Gbelcova, L. Muchova, K. Vanova, J. Zelenka, R. Konickova, J. Suk, M. Zadinova, Z. Knejzlik, S. Ahmad, T. Fujisawa, A. Ahmed, T. Ruml, Dig. Liver Dis., vol. 46, 2014, pp. 369-375.

[18] F. Zobi, Future Med. Chem., vol. 5, 2013, pp. 175-188.

[19] M.A. Wright, J.A. Wright, Dalton Trans., vol. 45, 2016, pp. 6801-6811.

[20] E. Kottelat, F. Zobi, Inorganics, vol. 5, 2017.

[21] M. Kourti, W.G. Jiang, J. Cai, Oxid. Med. Cell. Longev., vol. 2017, 2017, pp. 9326454.

[22] J. Jimenez, M.N. Pinto, J. Martinez-Gonzalez, P.K. Mascharak, Inorg. Chim. Acta, vol. 485, 2019, pp. 112-117.

[23] M.N. Pinto, I. Chakraborty, J. Jimenez, K. Murphy, J. Wenger, P.K. Mascharak, Inorg. Chem., vol. 58, 2019, pp. 14522-14531.

[24] M.N. Pinto, I. Chakraborty, C. Sandoval, P.K. Mascharak, J. Control. Release, vol. 264, 2017, pp. 192-202.

[25] I. Chakraborty, S.J. Carrington, G. Roseman, P.K. Mascharak, Inorg. Chem., vol. 56, 2017, pp. 1534-1545.

[26] S.J. Carrington, I. Chakraborty, P.K. Mascharak, Chem. Commun., vol. 49, 2013, pp. 11254-11256.

[27] S.J. Carrington, I. Chakraborty, J.M. Bernard, P.K. Mascharak, ACS Med. Chem. Lett., vol. 5, 2014, pp. 1324-1328.

[28] B. Kawahara, S. Ramadoss, G. Chaudhuri, C. Janzen, S. Sen, P.K. Mascharak, J. Inorg. Biochem., vol. 191, 2019, pp. 29-39.

[29] B. Kawahara, T. Moller, K. Hu-Moore, S. Carrington, K.F. Faull, S. Sen, P.K. Mascharak, J. Med. Chem., vol. 60, 2017, pp. 8000-8010.
[30] C.S. Jackson, S. Schmitt, Q.P. Dou, J.J. Kodanko, Inorg. Chem., vol. 50, 2011, pp. 5336-5338.
[31] J. Niesel, A. Pinto, H.W. Peindy N'Dongo, K. Merz, I. Ott, R. Gust, U. Schatzschneider, Chem. Commun., 2008, pp. 1798-1800.
[32] N.E. Bruckmann, M. Wahl, G.J. Reiss, M. Kohns, W. Watjen, P.C. Kunz, Eur. J. Inorg. Chem., 2011, pp. 4571-4577.
[33] E. Ustun, A. Ozgur, K.A. Coskun, S. Demir, I. Ozdemir, Y. Tutar, J. Coord. Chem., vol. 69, 2016, pp. 3384-3394.
[34] E. Ustun, A. Ozgur, K.A. Coskun, S.D. Dusunceli, I. Ozdemir, Y. Tutar, Transit. Met. Chem., vol. 42, 2017, pp. 331-337.
[35] A. Loboda, A. Jozkowicz, J. Dulak, Vascul. Pharmacol., vol. 74, 2015, pp. 11-22.
[36] C.C. Romão, H.L.A. Vieira, in: G. Jaouen, M. Salmain (Eds.), Bioorganometallic Chemistry, vol. 1, Wiley-VCH Verlag GmbH & Co. KGaA, 2014, pp. 165-202.
[37] I.C. Winburn, K. Gunatunga, R.D. McKernan, R.J. Walker, I.A. Sammut, J.C. Harrison, Basic Clin. Pharmacol. Toxicol., vol. 111, 2012, pp. 31-41.
[38] S.C. Marker, S.N. MacMillan, W.R. Zipfel, Z. Li, P.C. Ford, J.J. Wilson, Inorg. Chem., vol. 57, 2018, pp. 1311-1331.
[39] J. Rossier, D. Hauser, E. Kottelat, B. Rothen-Rutishauser, F. Zobi, Dalton Trans., vol. 46, 2017, pp. 2159-2164.
[40] M. Chrominski, A. Lewalska, D. Gryko, Chem. Commun., vol. 49, 2013, pp. 11406-11408.
[41] G. Santoro, T. Zlateva, A. Ruggi, L. Quaroni, F. Zobi, Dalton Trans., vol. 44, 2015, pp. 6999-7008.
[42] P. Govender, S. Pai, U. Schatzschneider, G.S. Smith, Inorg. Chem., vol. 52, 2013, pp. 5470-5478.
[43] E. Kottelat, F. Lucarini, A. Crochet, A. Ruggi, F. Zobi, Eur. J. Inorg. Chem., vol. 2019, 2019, pp. 3758-3768.
[44] M. Ruetz, R. Salchner, K. Wurst, S. Fedosov, B. Kräutler, Angew. Chem. Int. Ed., vol. 52, 2013, pp. 11406-11409.
[45] P. Ruiz-Sanchez, C. Konig, S. Ferrari, R. Alberto, J. Biol. Inorg. Chem., vol. 16, 2011, pp. 33-44.
[46] A.R. Vortherms, A.R. Kahkoska, A.E. Rabideau, J. Zubieta, L.L. Andersen, M. Madsen, R.P. Doyle, Chem. Commun., vol. 47, 2011, pp. 9792-9794.
[47] S.N. Fedosov, C.B. Grissom, N.U. Fedosova, S.K. Moestrup, E. Nexø, T.E. Petersen, FEBS J., vol. 273, 2006, pp. 4742-4753.
[48] A. Loboda, A. Jozkowicz, J. Dulak, Thromb. Haemost., vol. 114, 2015, pp. 432-433.
[49] I. Naletova, C. Satriano, A. Curci, N. Margiotta, G. Natile, G. Arena, D. La Mendola, V.G. Nicoletti, E. Rizzarelli, Oncotarget, vol. 9, 2018, pp. 36289-36316.
[50] N.S. Ng, M.J. Wu, J.R. Aldrich-Wright, J. Inorg. Biochem., vol. 180, 2018, pp. 61-68.
[51] A. Gil, A. Sanchez-Gonzalez, V. Branchadell, J. Chem. Inf. Model., vol. 59, American Chemical Society, 2019, pp. 3989-3995.
[52] L.S. Nobre, J.D. Seixas, C.C. Romao, L.M. Saraiva, Antimicrob. Agents Chemother., vol. 51, 2007, pp. 4303-4307.
[53] J.L. Wilson, H.E. Jesse, B. Hughes, V. Lund, K. Naylor, K.S. Davidge, G.M. Cook, B.E. Mann, R.K. Poole, Antioxid. Redox Signal., vol. 19, 2013, pp. 497-509.
[54] J.L. Wilson, L.K. Wareham, S. McLean, R. Begg, S. Greaves, B.E. Mann, G. Sanguinetti, R.K. Poole, Antioxid. Redox Signal., vol. 23, 2015, pp. 148-162.

[55] M. Desmard, R. Foresti, D. Morin, M. Dagouassat, A. Berdeaux, E. Denamur, S.H. Crook, B.E. Mann, D. Scapens, P. Montravers, J. Boczkowski, R. Motterlini, Antioxid. Redox Signal., vol. 16, 2012, pp. 153-163.
[56] A.F. Tavares, M.R. Parente, M.C. Justino, M. Oleastro, L.S. Nobre, L.M. Saraiva, Plos One, vol. 8, 2013, pp. e83157.
[57] N. Rana, S. McLean, B.E. Mann, R.K. Poole, Microbiology, vol. 160, 2014, pp. 2771-2779.
[58] H.M. Southam, T.W. Smith, R.L. Lyon, C. Liao, C.R. Trevitt, L.A. Middlemiss, F.L. Cox, J.A. Chapman, S.F. El-Khamisy, M. Hippler, M.P. Williamson, P.J.F. Henderson, R.K. Poole, Redox Biol., vol. 18, 2018, pp. 114-123.
[59] S. McLean, B.E. Mann, R.K. Poole, Anal. Biochem., vol. 427, 2012, pp. 36-40.
[60] G. Santoro, R. Beltrami, E. Kottelat, O. Blacque, A.Y. Bogdanova, F. Zobi, Dalton Trans., vol. 45, 2016, pp. 1504-1513.
[61] N. Rana, H.E. Jesse, M. Tinajero-Trejo, J.A. Butler, J.D. Tarlit, M.L. von Und Zur Muhlen, C. Nagel, U. Schatzschneider, R.K. Poole, Microbiology, vol. 163, 2017, pp. 1477-1489.
[62] C. Bisig, A. Petri-Fink, B. Rothen-Rutishauser, Inhal. Toxicol., vol. 30, 2018, pp. 40-48.
[63] A. Baron, C. Herrero, A. Quaranta, M.F. Charlot, W. Leibl, B. Vauzeilles, A. Aukauloo, Inorg. Chem., vol. 51, 2012, pp. 5985-5987.
[64] R. Ziessel, J. Suffert, M.T. Youinou, J. Org. Chem., vol. 61, 1996, pp. 6535-6546.
[65] V.M. Mukkala, J.J. Kankare, Helv. Chim. Acta, vol. 75, 1992, pp. 1578-1592.

SUPPORTING INFORMATION FOR

Cytotoxicity of Mn-based photoCORMs of ethynyl-α-diimine ligands against different cancer cell lines: The key role of CO-depleted metal fragments

Jeremie Rossier[†], Joachim Delasoie[†], Laetitia Häni[‡], Daniel Hauser[‡], Barbara Rothen-Rutishauser[‡] and Fabio Zobi*[,†]

† Department of Chemistry, University of Fribourg, Chemin du Musée 9, 1700 Fribourg, Switzerland
‡ Adolphe Merkle Institute, Chemin des Verdiers 4, 1700 Fribourg, Switzerland

*To whom all the correspondence should be addressed.

Phone (+41) 26 300 87 85, Fax (+41) 26 300 97 37, E-mail : fabio.zobi@unifr.ch

NMR Spectra

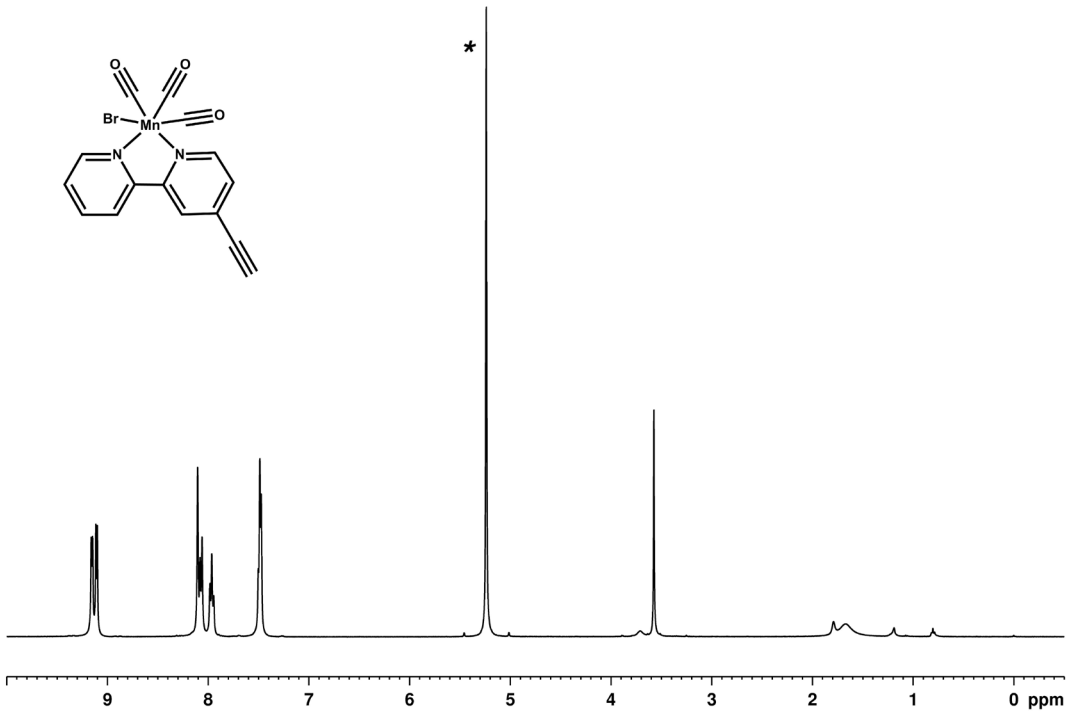

Figure S1. 500 MHz ^{1}H-NMR of compound Mn-**1** (in CD_2Cl_2, ✱= solvent residual peak)

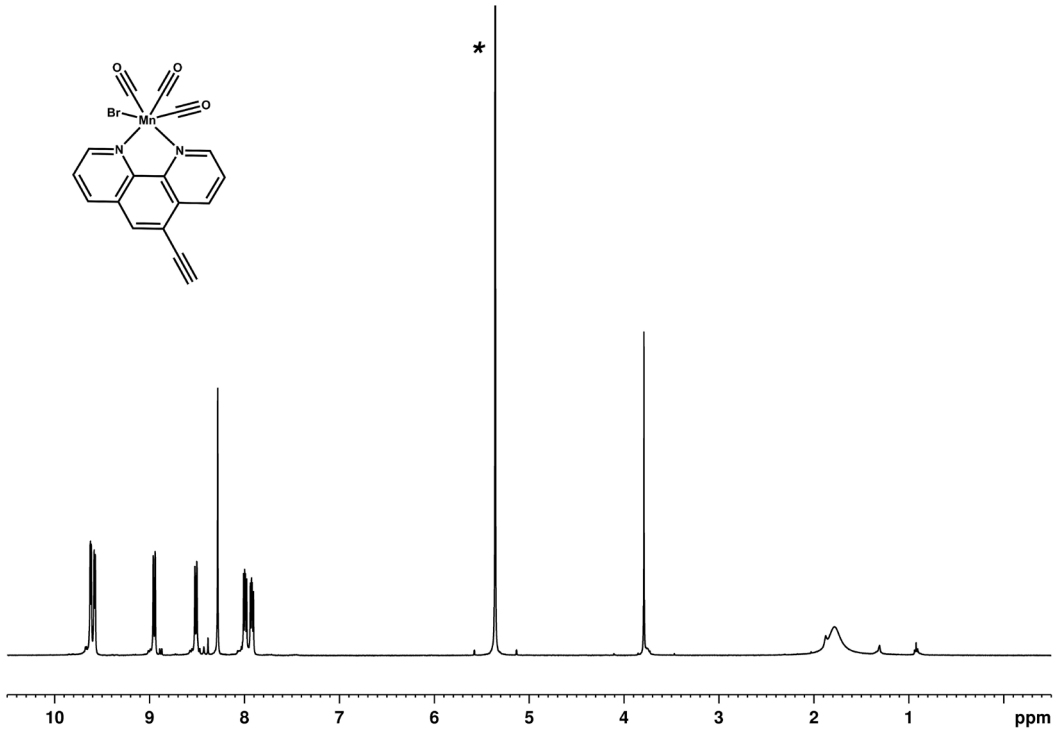

Figure S2. 500 MHz ^{1}H-NMR of compound Mn-**2** (in CD_2Cl_2, ✱= solvent residual peak)

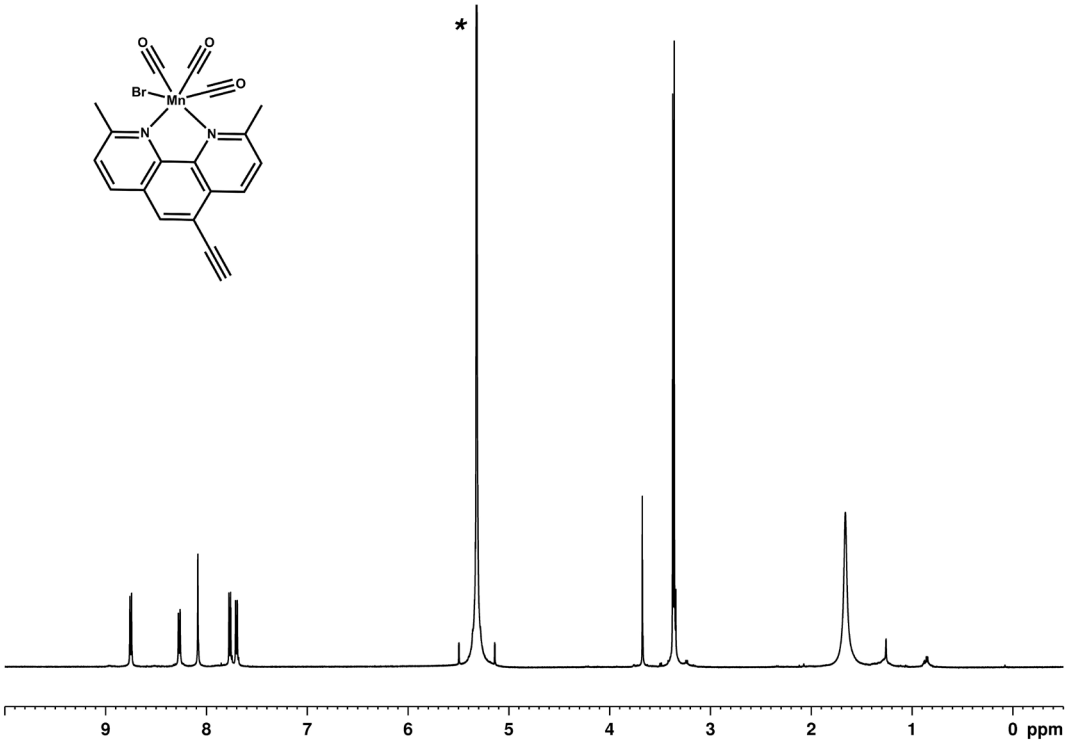

Figure S3. 500 MHz ^{1}H-NMR of compound Mn-**3** (in CD_2Cl_2, ✱= solvent residual peak)

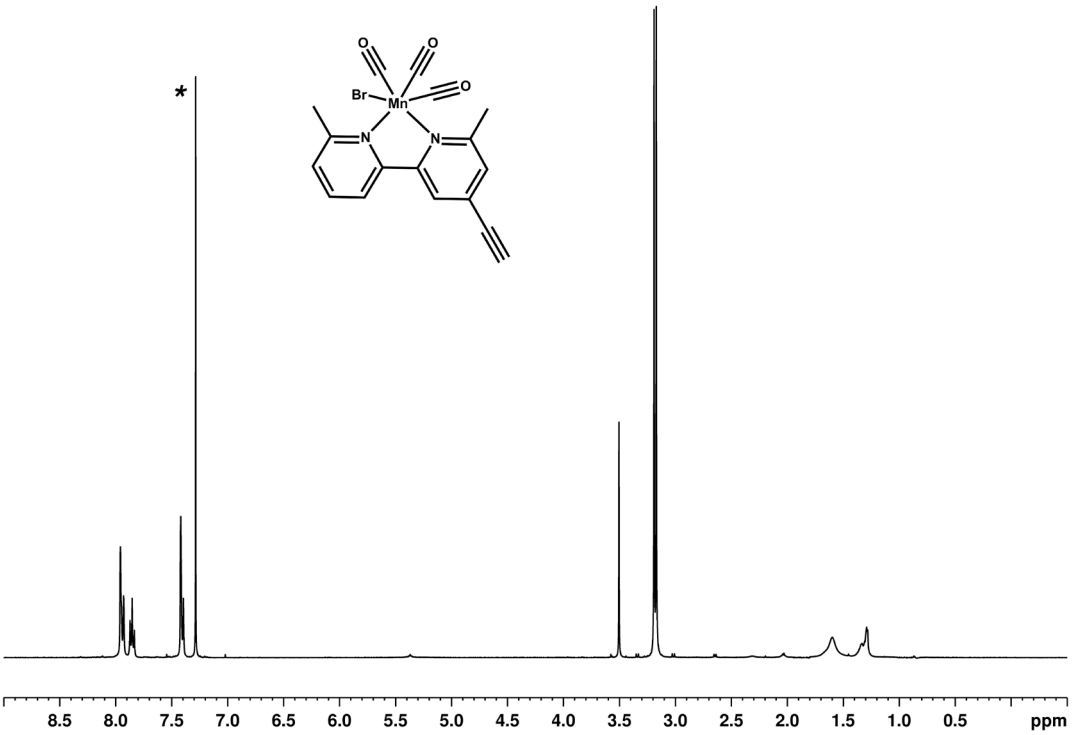

Figure S4. 500 MHz ^{1}H-NMR of compound Mn-**4** (in $CDCl_3$, ✱= solvent residual peak)

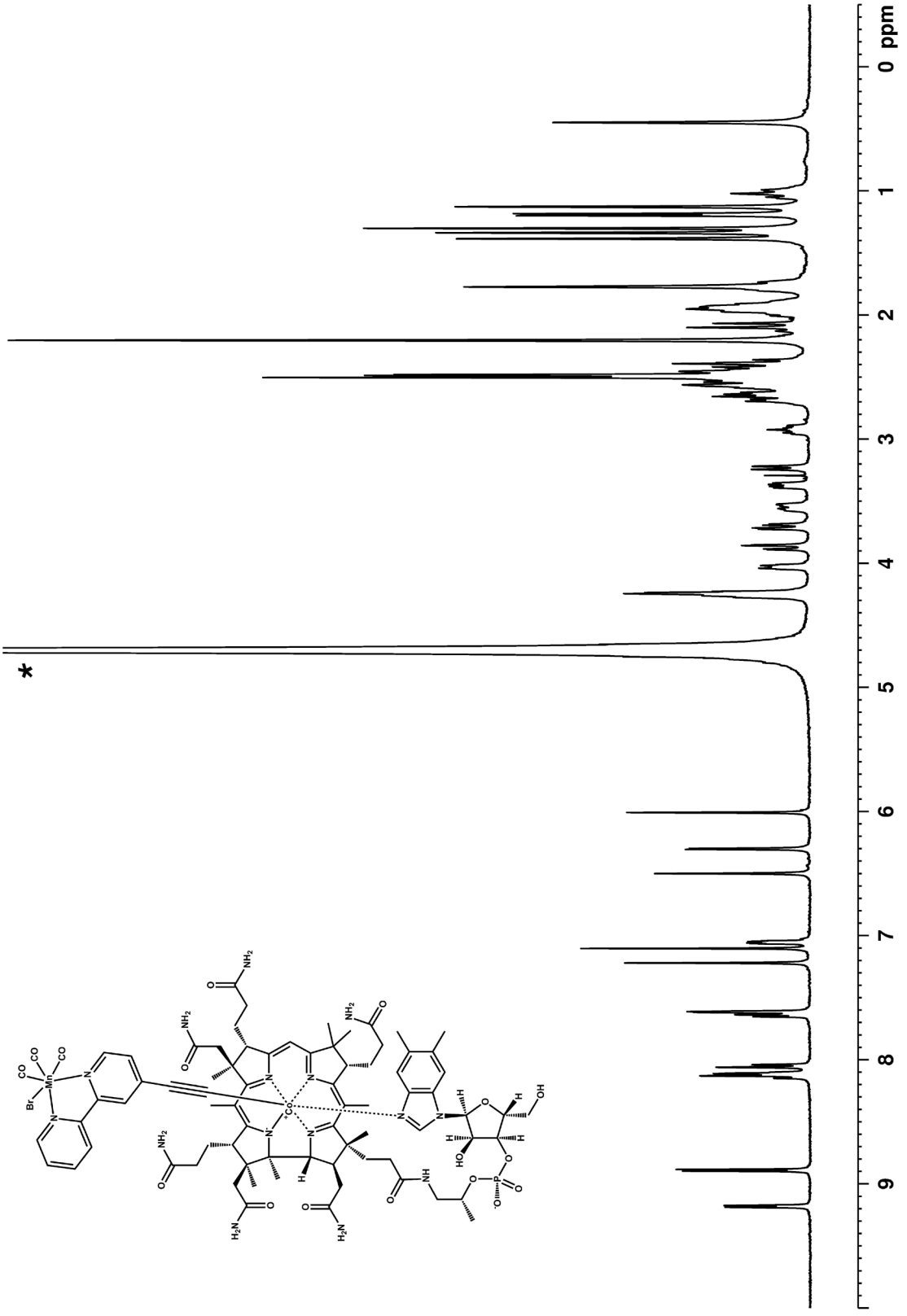

Figure S5. 500 MHz ^{1}H-NMR of compound B_{12}-Mn-**1** (in D_2O, ✱= solvent residual peak)

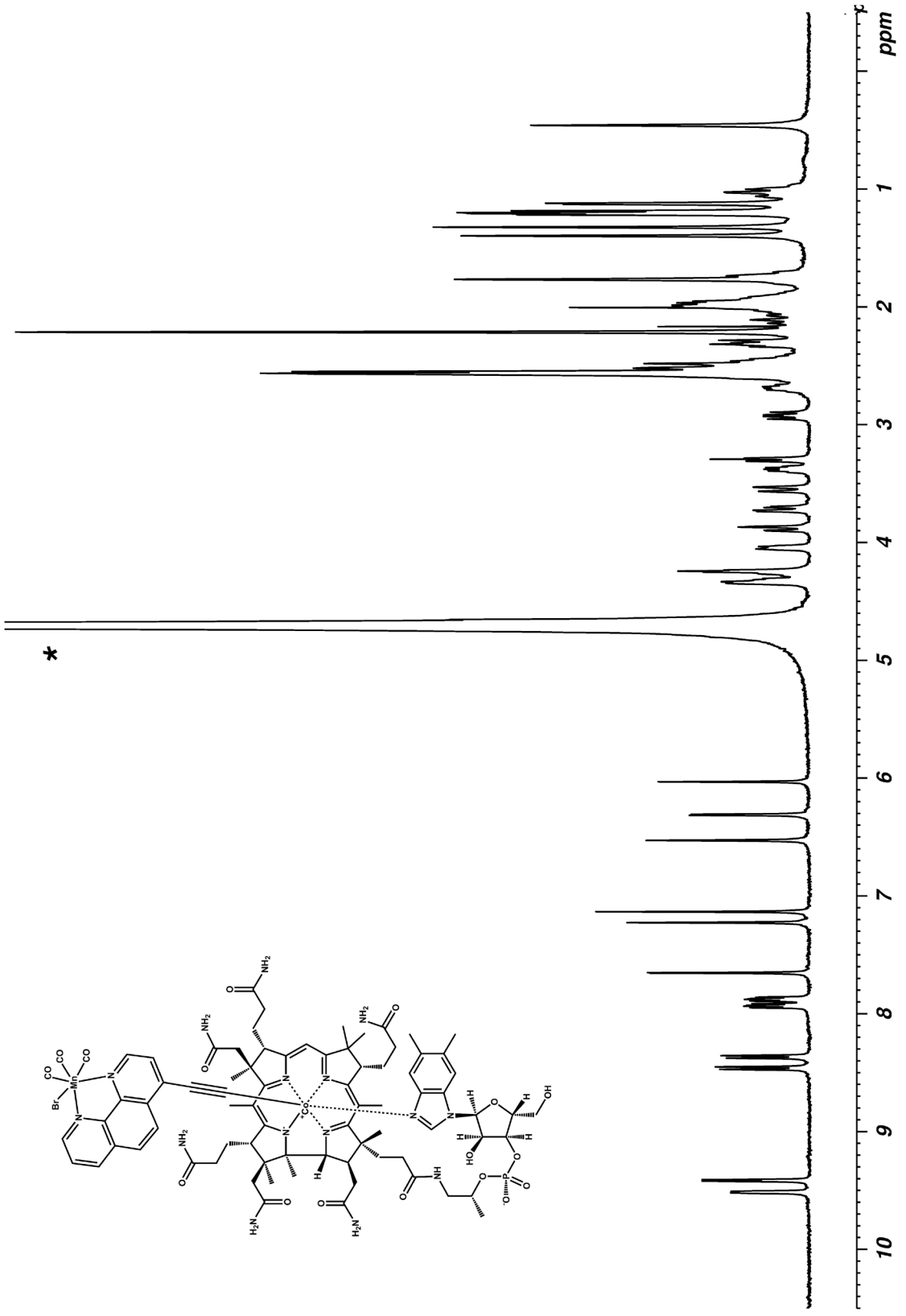

Figure S6. 500 MHz ^{1}H-NMR of compound B_{12}-Mn-**2** (in D_2O, ✱= solvent residual peak)

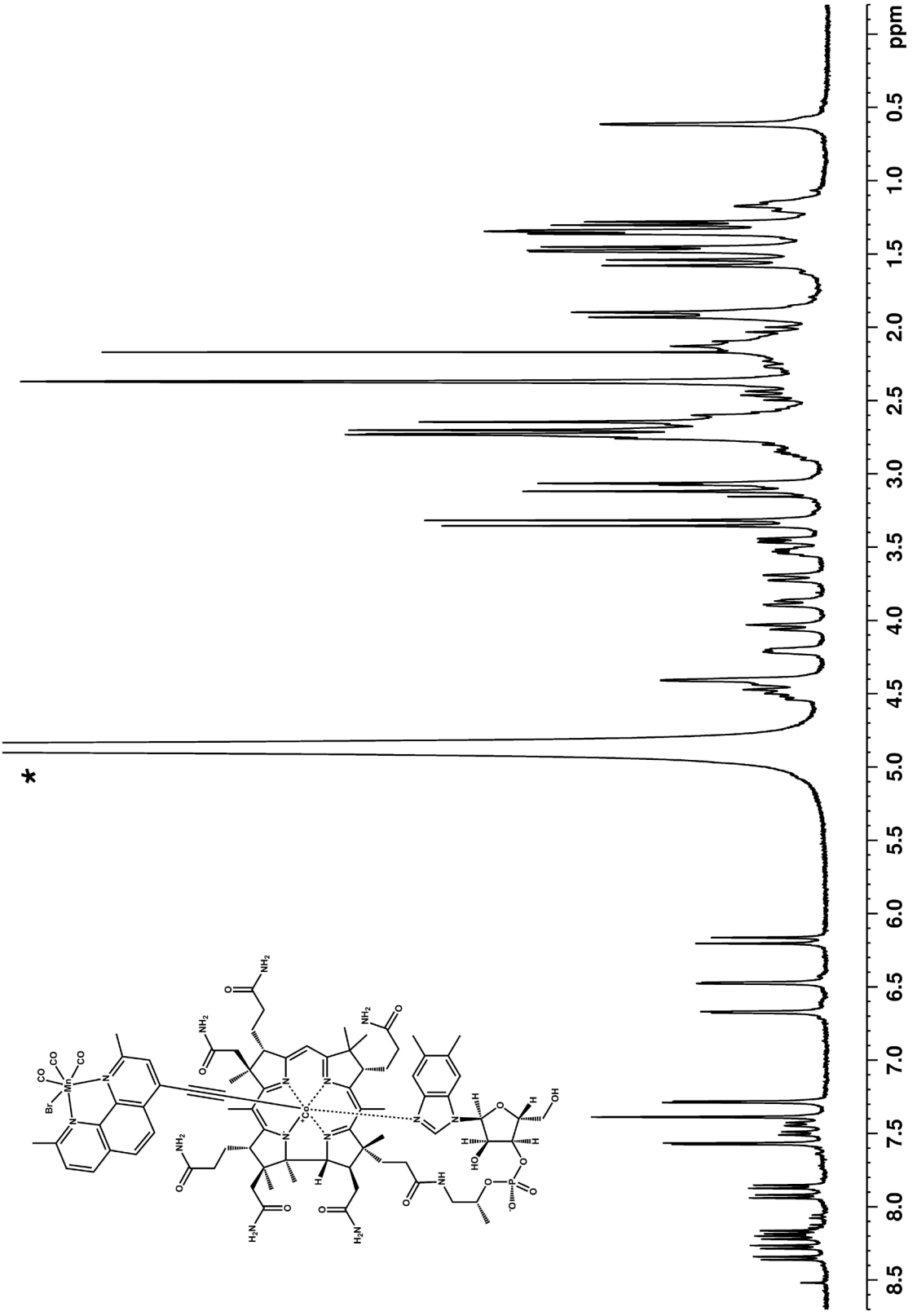

Figure S7. 500 MHz ^{1}H-NMR of compound B_{12}-Mn-**3** (in D_2O, ✱= solvent residual peak)

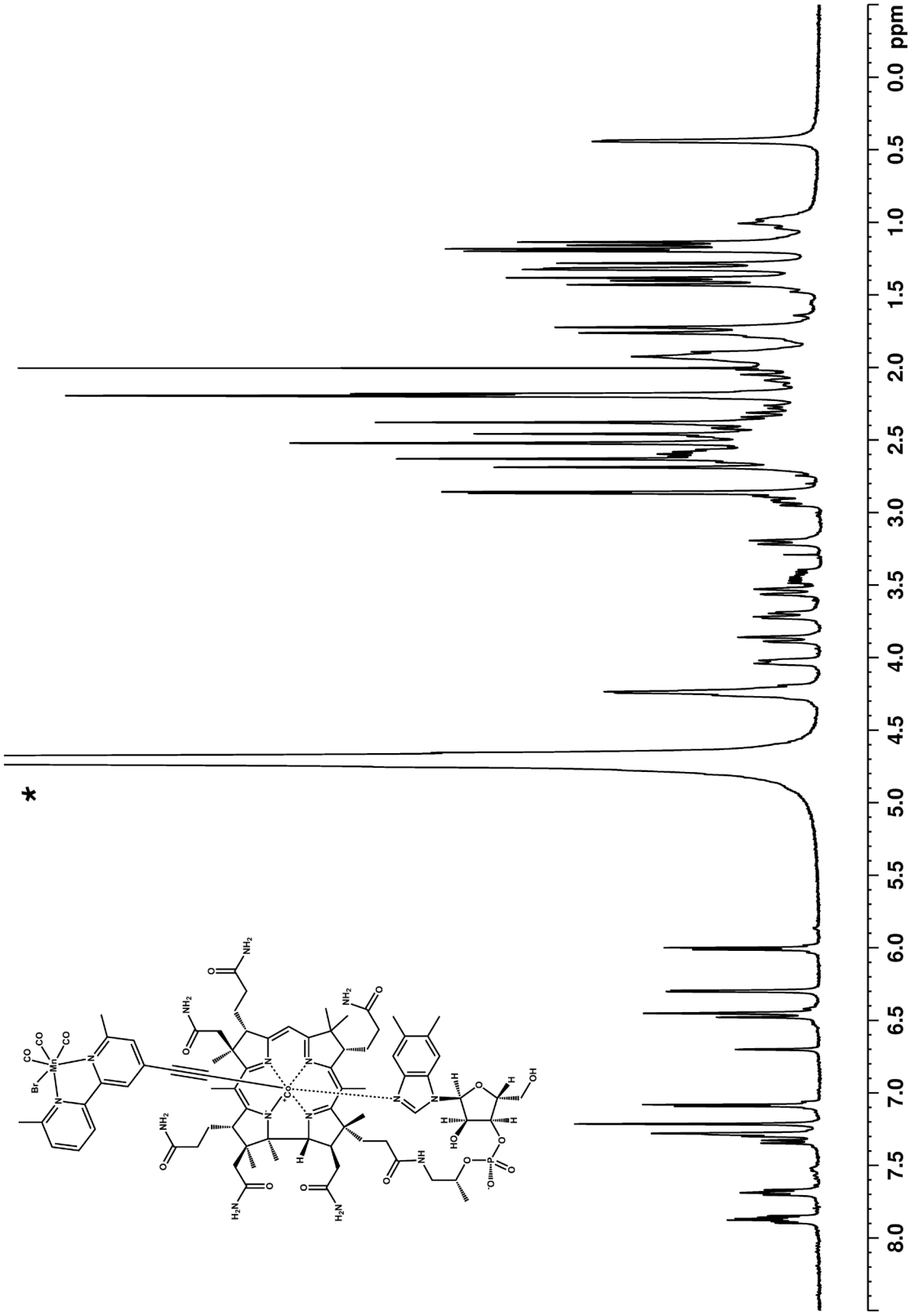

Figure S8. 500 MHz ^{1}H-NMR of compound B_{12}-Mn-**4** (in D_2O, ✱= solvent residual peak)

Equivalent of CO released

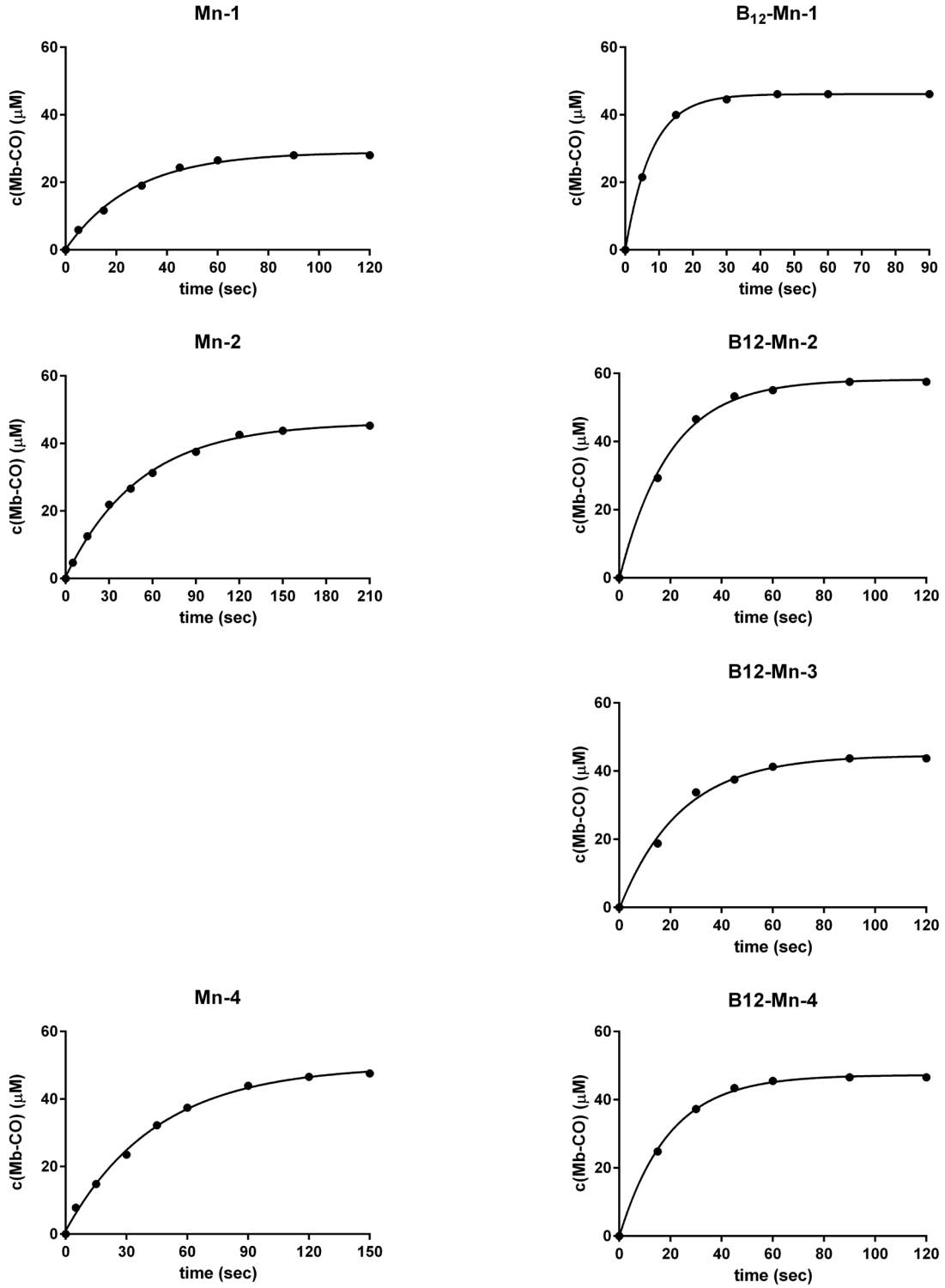

Figure S9. Amount of Mb-CO in µM formed with increasing irradiation time at 420 nm for solutions of compounds Mn-**1** to -**4** and B_{12}-Mn-**1** to -**4** (20 µM) in 0.1 M PBS at pH 7.4 in the presence of myoglobin (60 µM) and sodium dithionite (10 mM) under a dinitrogen atmosphere as determined from UV/vis spectroscopy. The complexes Mn-**1**, -**2** and -**4** were previously dissolved in DMSO (1% final concentration) while Mn-**3** could not be tested due to its poor solubility.

Half-life

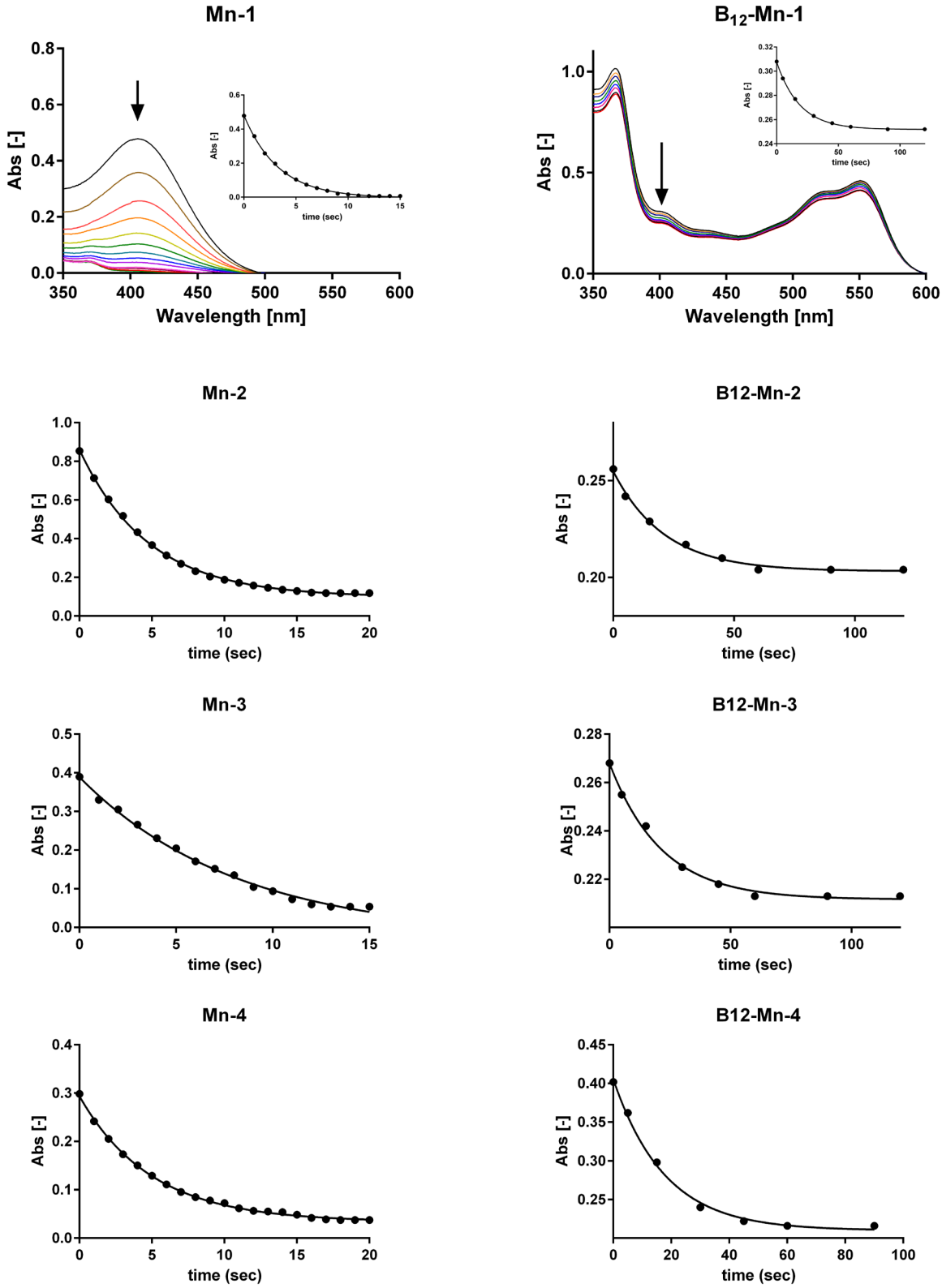

Figure S10. Monitoring of the spectral changes in the electronic absorption spectrum of compounds Mn-**1** to -**4** and B_{12}-Mn-**1** to -**4** in 0.1 M PBS upon irradiation with 420 nm light. The complexes Mn-**1**, -**2** and -**4** were previously dissolved in DMSO (1% final concentration) while Mn-**3** was tested in methanol.

UV-Vis spectra

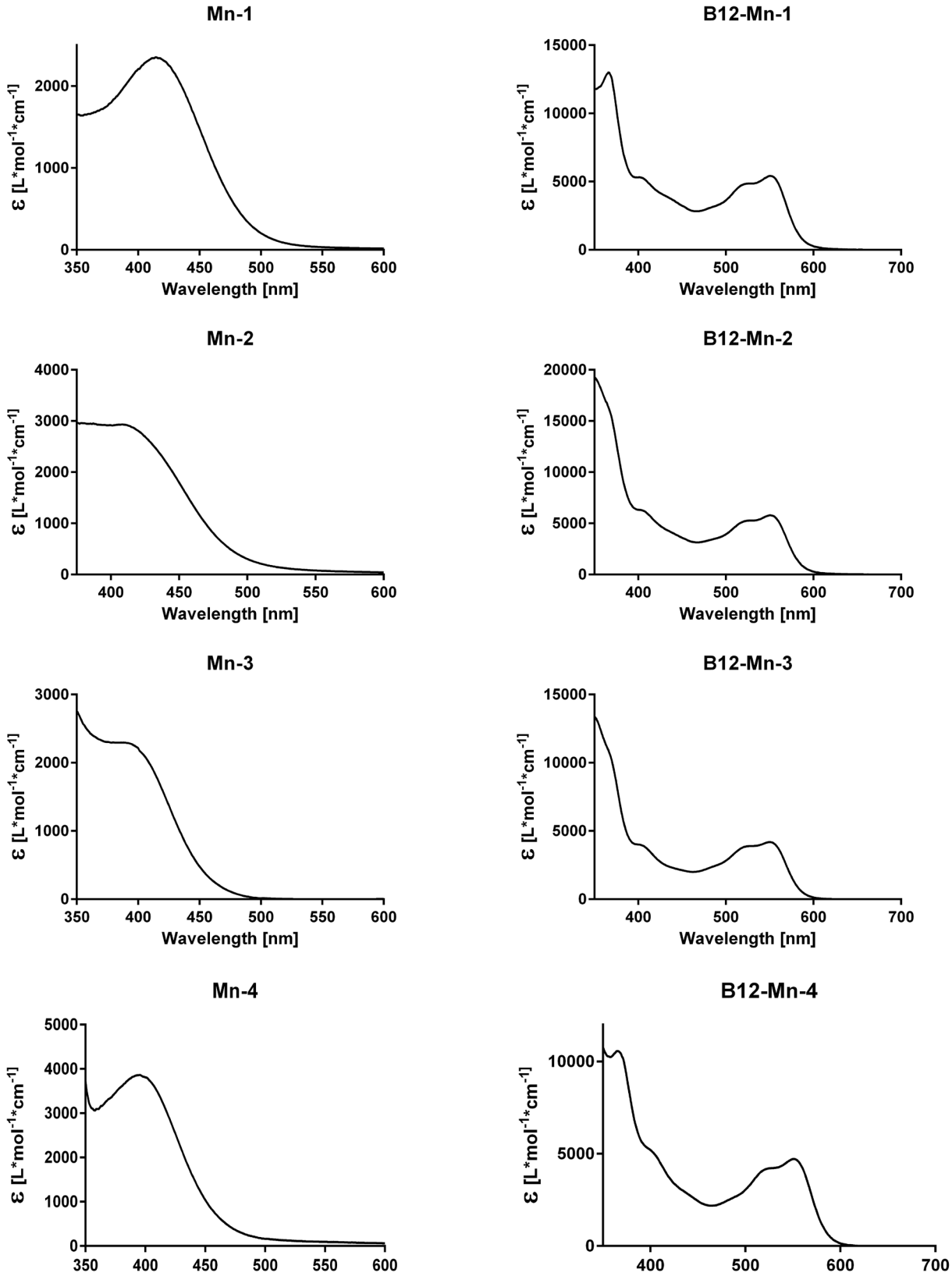

Figure S11. UV-Vis spectra of compounds Mn-1 to -4 (in methanol) and B12-Mn-**1** to -**4** (in 0.1M PBS)

Crystallographic details

Table S1: Crystal data and structure refinement for Mn-**1**

Empirical formula	$C_{15}H_8BrMnN_2O_3$
Formula weight	399.08
Temperature	100.00(10) K
Crystal system	monoclinic
Space group	*P*21/*c*
Unit cell dimensions	a = 7.3490(5) Å
	b = 9.1242(6) Å
	c = 12.5779(9) Å
Unit cell dimensions	α = 7.3490(5) Å
	β = 9.1242(6) Å
	γ = 12.5779(9) Å
Volume/Å^3	1463.6(2)
Z	4
Density (calculated)	1.811 Mg/m^3
Absorbtion coefficient	10.662 mm^{-1}
F(000)	784.0
Crystal size	0.190 × 0.141 × 0.055 mm^3
Radiation	Cu Kα (λ = 1.54184)
2*Θ* range for data collection/°	10.356 to 151.622
Index ranges	-16 ≤ h ≤ 18, -13 ≤ k ≤ 10, -11 ≤ l ≤ 11
Reflections collected	9952
Independent reflections	2981 [R_{int} = 0.0633, R_{sigma} = 0.0611]
Data/restraints/parameters	2981/2/203
Goodness-of-fit on F^2	1.031
Final *R* indexes [I > 2σ (I)]	R_1 = 0.0486, wR_2 = 0.1187
Final *R* indexes [all data]	R_1 = 0.0744, wR_2 = 0.1304
Largest diff. peak and hole	0.82/-0.95 e.Å^{-3}

Table S2: Crystal data and structure refinement for Mn-**2**.

Empirical formula	$C_{17}H_8BrMnN_2O_3$	
Formula weight	423.10	
Temperature	100.00(10) K	
Wavelength	1.54184 Å	
Crystal system	Triclinic	
Space group	$P\bar{1}$	
Unit cell dimensions	a = 7.3490(5) Å	α= 71.174(6)°.
	b = 9.1242(6) Å	β= 79.887(6)°.
	c = 12.5779(9) Å	γ = 81.860(6)°.
Volume	782.60(10) Å^3	
Z	2	
Density (calculated)	1.795 Mg/m^3	
Absorption coefficient	10.016 mm^{-1}	
F(000)	416	
Crystal size	0.265 x 0.233 x 0.029 mm^3	
Radiation	Cu Kα (λ = 1.54184)	
ϑ range for data collection	3.749 to 75.681°.	
Index ranges	-8 ≤ h ≤ 5, -11 ≤ k ≤ 10, -15 ≤ l ≤ 14	
Reflections collected	5217	
Independent reflections	3124 [R_{int} = 0.0317]	
Completeness to ϑ = 67.684°	99.9 %	
Absorption correction	Gaussian	
Max. and min. transmission	1.000 and 0.172	
Refinement method	Full-matrix least-squares on F^2	
Data / restraints / parameters	3124 / 2 / 217	
Goodness-of-fit on F^2	1.049	
Final R indices [I>2σ(I)]	R_1 = 0.0488, wR_2 = 0.1316	
R indices (all data)	R_1 = 0.0555, wR_2 = 0.1389	
Largest diff. peak and hole	1.126 and -0.734 e.Å^{-3}	

Table S3: Crystal data and structure refinement for Mn-**3**

Empirical formula	$C_{19}H_{12}BrMnN_2O_3$	
Formula weight	451.16	
Temperature	100.00(10) K	
Wavelength	1.54184 Å	
Crystal system	Monoclinic	
Space group	P21/c	
Unit cell dimensions	a = 12.4157(6) Å	α= 90°.
	b = 10.8348(5) Å	β= 94.772(5)°.
	c = 12.8562(8) Å	γ = 90°.
Volume	1723.45(16) $Å^3$	
Z	4	
Density (calculated)	1.739 Mg/m^3	
Absorption coefficient	9.138 mm^{-1}	
F(000)	896	
Crystal size	0.203 x 0.199 x 0.070 mm3	
θ range for data collection	3.572 to 76.195°.	
Index ranges	-15 ≤ h ≤ 12, -10 ≤ k ≤ 13, -16 ≤ l ≤ 15	
Reflections collected	10459	
Independent reflections	3501 [Rint = 0.0535]	
Completeness to θ = 67.684°	99.4 %	
Absorption correction	Gaussian	
Max. and min. transmission	0.838 and 0.252	
Refinement method	Full-matrix least-squares on F2	
Data / restraints / parameters	3501 / 0 / 237	
Goodness-of-fit on F^2	1.047	
Final R indices [I>2σ(I)]	R1 = 0.0548, wR2 = 0.1413	
R indices (all data)	R1 = 0.0603, wR2 = 0.1492	
Largest diff. peak and hole	1.542 and -0.844 e.Å-3	

Table S4: Crystal data and structure refinement for Mn-**4**.

Empirical formula	$C_{17}H_{12}BrMnN_2O_3$
Formula weight	427.14
Temperature	100.00(10) K
Crystal system	triclinic
Space group	$P\bar{1}$
Unit cell dimensions	a = 7.7032(3) Å
	b = 8.5452(4) Å
	c = 12.3936(5) Å
Unit cell dimensions	α = 81.123(4) Å
	β = 84.120(3) Å
	γ = 81.292(3) Å
Volume/Å^3	794.14(6)
Z	2
Density (calculated)	1.786 Mg/m^3
Absorbtion coefficient	9.871 mm^{-1}
F(000)	424.0
Crystal size	0.400 × 0.241 × 0.126 mm^3
Radiation	Cu Kα (λ = 1.54184)
2Θ range for data collection/°	7.242 to 150.676
Index ranges	-5 ≤ h ≤ 9, -10 ≤ k ≤ 10, -15 ≤ l ≤ 15
Reflections collected	5429
Independent reflections	3175 [R_{int} = 0.0198, R_{sigma} = 0.0248]
Data/restraints/parameters	3175/1/229
Goodness-of-fit on F^2	1.089
Final *R* indexes [I>=2σ (I)]	R_1 = 0.0298, wR_2 = 0.0771
Final *R* indexes [all data]	R_1 = 0.0304, wR_2 = 0.0775
Largest diff. peak and hole	1.03/-0.54 e.Å^{-3}

Table S5: Crystal data and structure refinement for B_{12}-**bpy**.

Empirical formula	$C_{74}H_{111}CoN_{15}O_{22}P$	
Formula weight	1652.67	
Temperature	100.00(10) K	
Wavelength	0.71073 Å	
Crystal system	Orthorhombic	
Space group	P212121	
Unit cell dimensions	a = 15.7084(3) Å	α= 90°.
	b = 22.2447(5) Å	β= 90°.
	c = 25.5612(6) Å	γ = 90°.
Volume	8931.8(3) $Å^3$	
Z	4	
Density (calculated)	1.229 Mg/m3	
Absorption coefficient	0.284 mm^{-1}	
F(000)	3512	
Crystal size	0.453 x 0.147 x 0.117 mm3	
θ range for data collection	2.560 to 29.665°.	
Index ranges	-20 ≤ h ≤ 19, -30 ≤ k ≤ 20, -34 ≤ l ≤ 35	
Reflections collected	78051	
Independent reflections	22567 [Rint = 0.0378]	
Completeness to θ = 25.242°	99.8 %	
Absorption correction	Gaussian	
Max. and min. transmission	1.000 and 0.644	
Refinement method	Full-matrix least-squares on F2	
Data / restraints / parameters	22567 / 31 / 1083	
Goodness-of-fit on F2	1.025	
Final R indices [I>2σ(I)]	R1 = 0.0504, wR2 = 0.1196	
R indices (all data)	R1 = 0.0677, wR2 = 0.1282	
Absolute structure parameter	-0.009(4)	
Largest diff. peak and hole	0.623 and -0.420 e.Å-3	

Additional supporting images

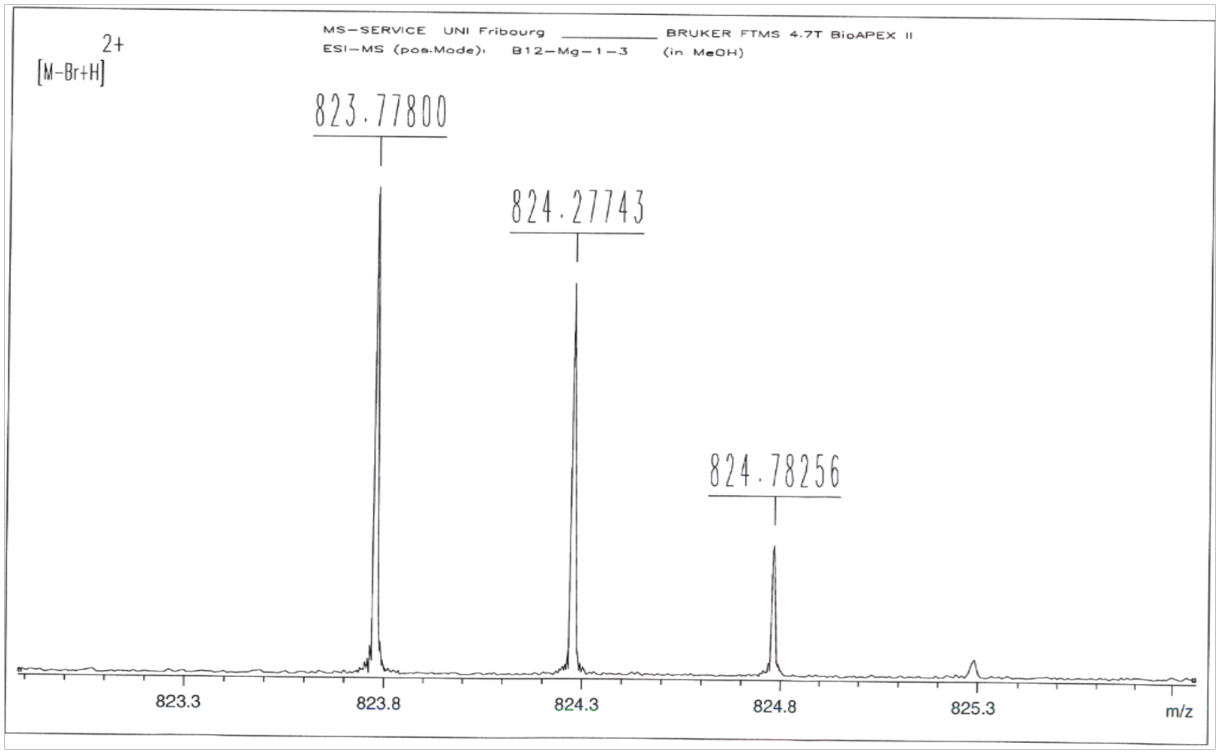

Figure S12: HR-ESI-MS spectrum (in MeOH) of compound B_{12}-Mn-**1**

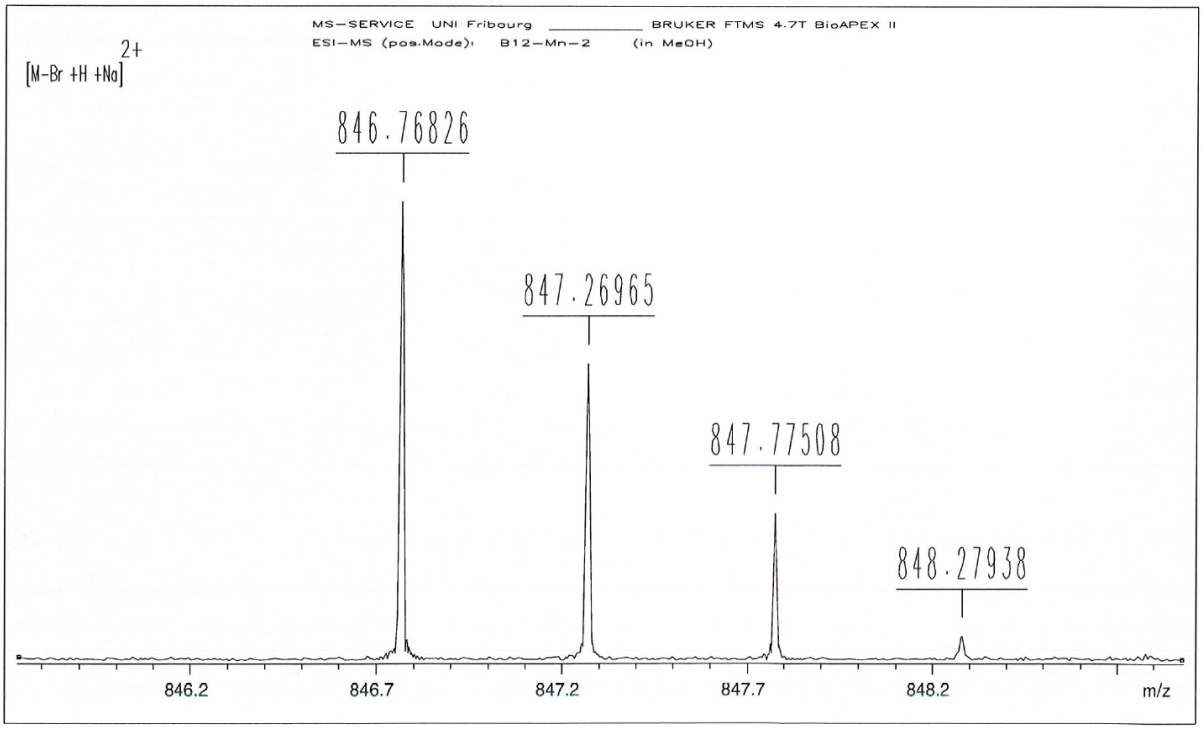

Figure S13: HR-ESI-MS spectrum (in MeOH) of compound B_{12}-Mn-**2**

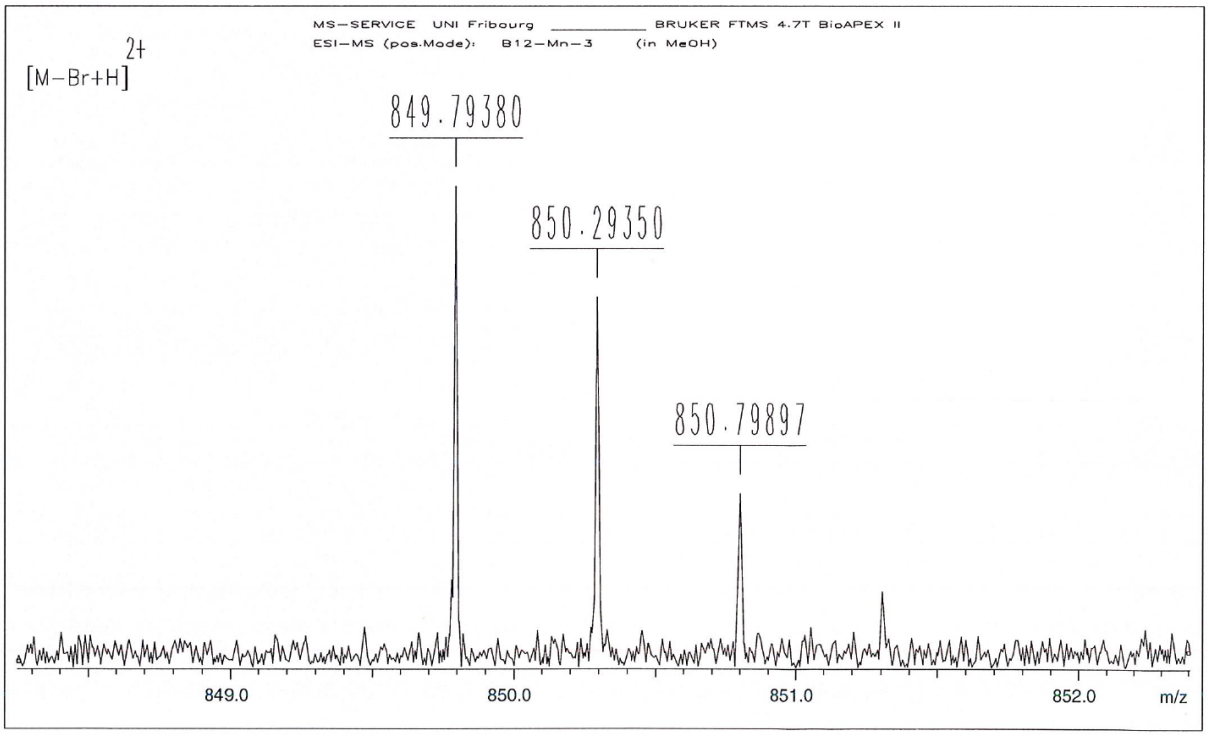

Figure S14: HR-ESI-MS spectrum (in MeOH) of compound B_{12}-Mn-**3**

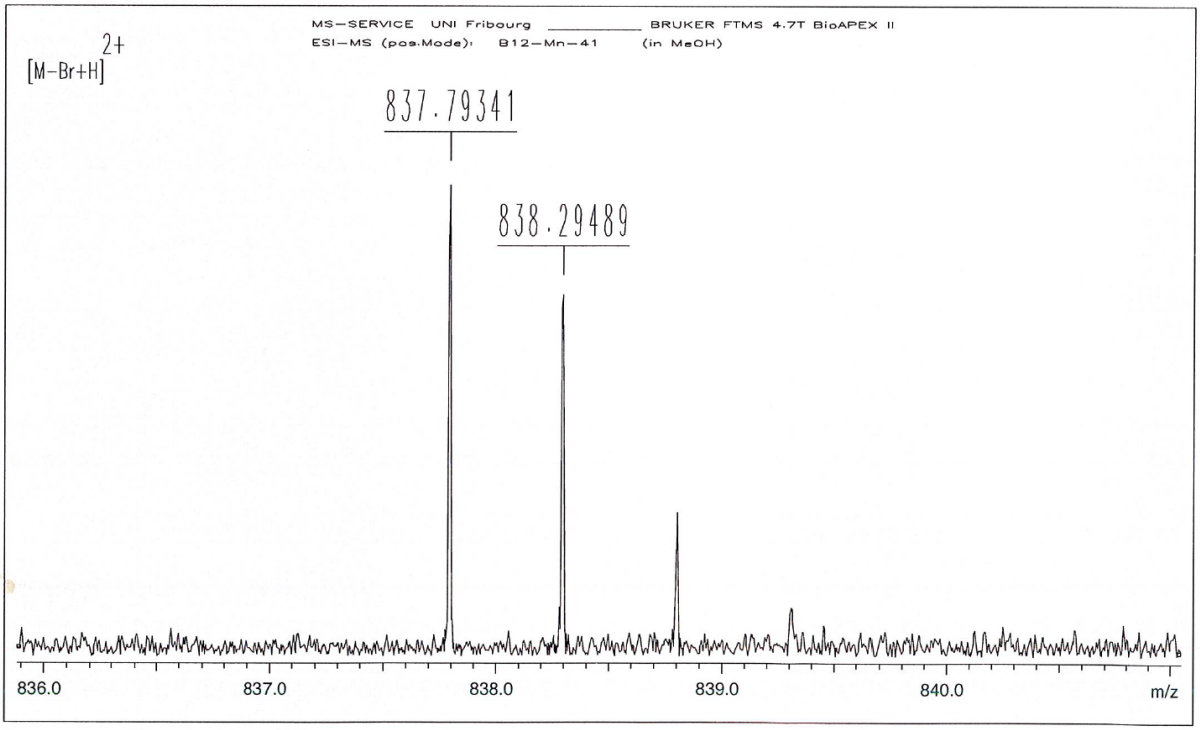

Figure S15: HR-ESI-MS spectrum (in MeOH) of compound B_{12}-Mn-**4**

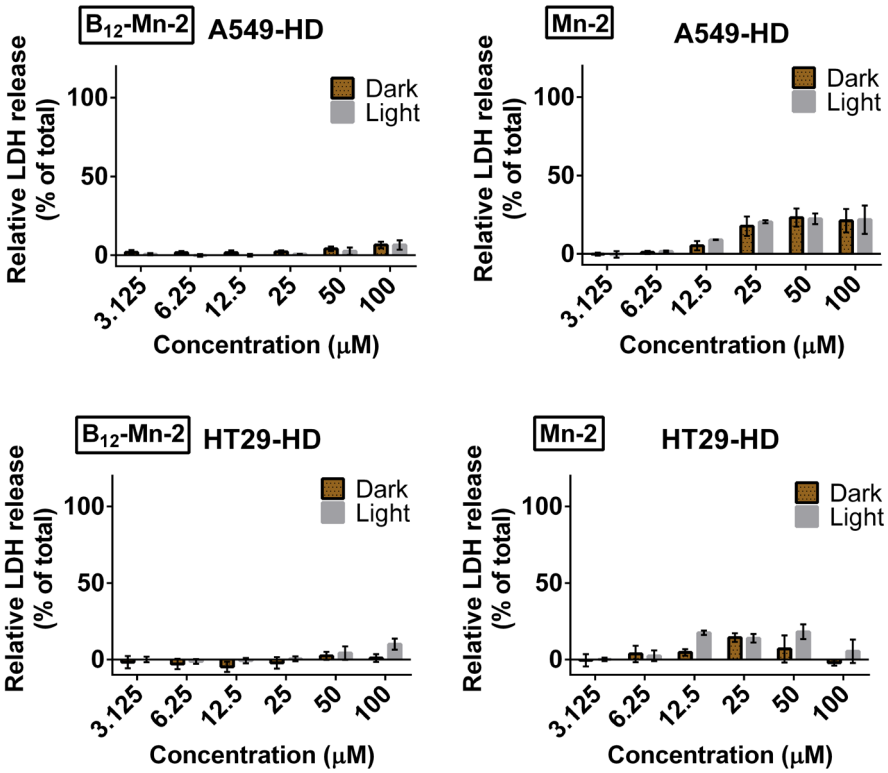

Figure S16: Graphs illustrating levels of LDH relative to the positive control (Triton X)

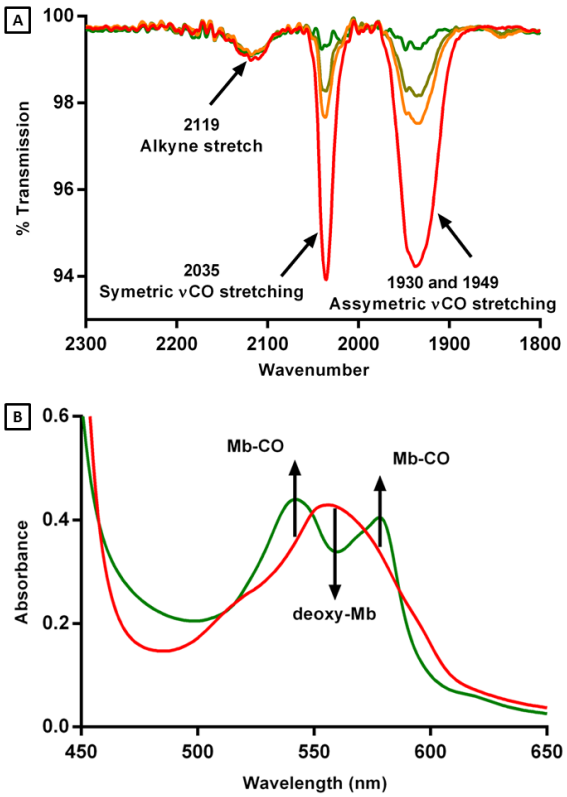

Figure S17: Typical CO releasing experiment. (A) IR spectrum of compound B_{12}-Mn-**4** in methanol following 20 seconds time lapses of irradiation (B) conversion of deoxy-Mb to Mb-CO by B_{12}-Mn-**4** under the myoglobin assay condition.

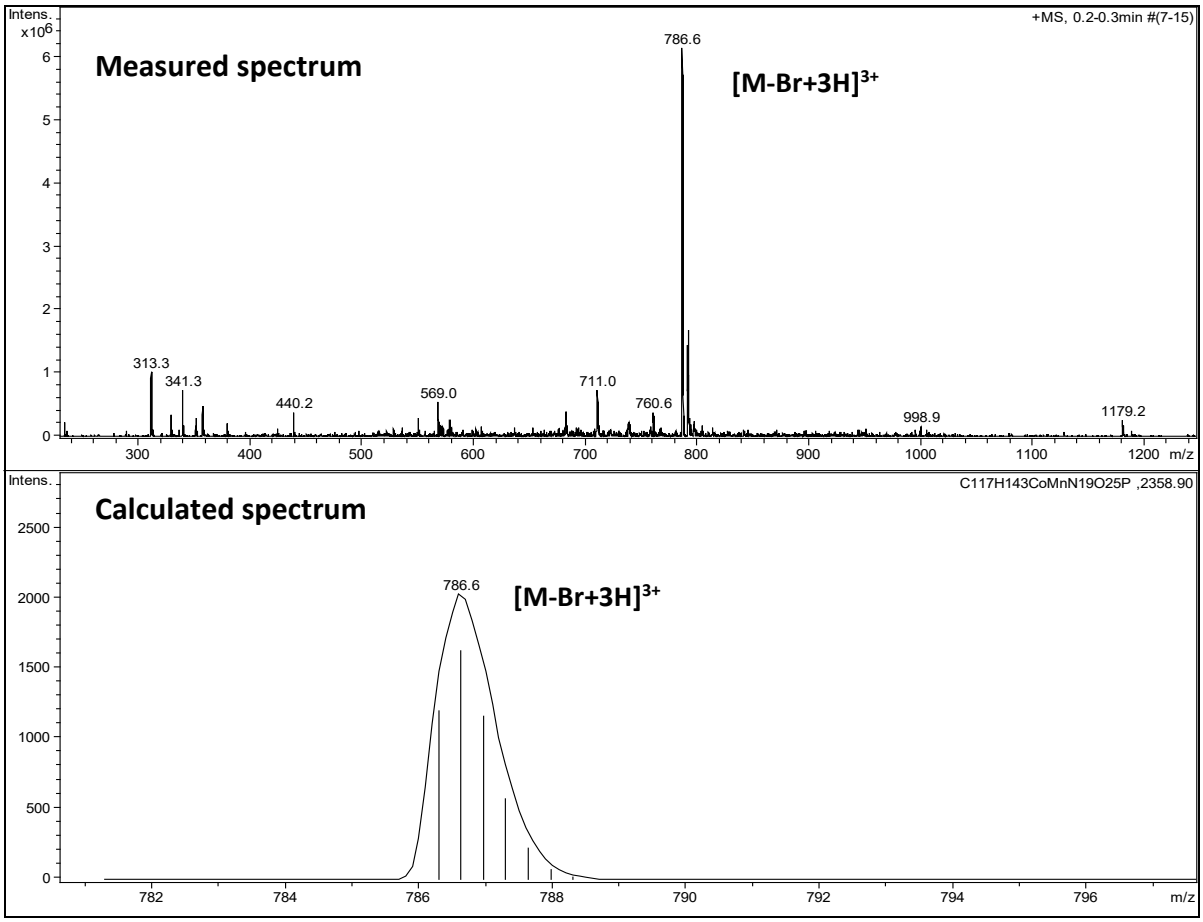

Figure S18: Mass spectrum of compound B_{12}Mn-**2**

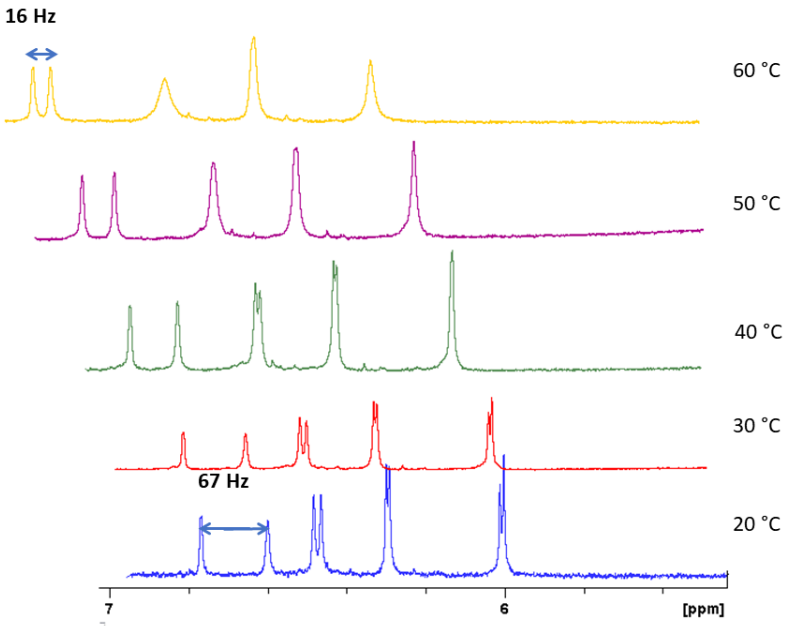

Figure S19: Temperature-dependent measurements of compound B_{12}-Mn-**4** showing the coalescence of split aromatic signals belonging to the same proton as evidence of the presence of two conformations at the upper ligand of the derivative.

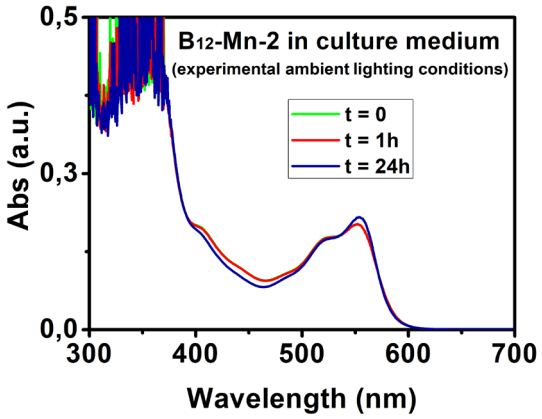

Figure S20: Spectral changes in the electronic absorption spectrum of B12-Mn-**2** incubated in cell culture medium and exposed to experimental ambient light conditions over the course of 24h.